Disformal Quintessence: Observational constraints and linear perturbations

Memoria de trabajo presentada por **Miguel Zumalacárregui Pérez**
para optar al titulo de **Máster en Física Téorica** por la
Universidad Autónoma de Madrid

Trabajo tutelado por **Dra. Pilar Ruiz-Lapuente**
Profesora titular del Departamento de Astronomía y
Meteorología de la Universidad de Barcelona,

Dr. David Fonseca Mota
Investigador titular del Instituto de Astrofísica
Teórica de la Universidad de Oslo,

y **Dr. Juan Garcia-Bellido**
Profesor titular del Departamento de Física Teórica
de la Universidad Autónoma de Madrid

Departamento de Física Teórica, Universidad Autónoma de Madrid
Instituto de Física Teórica, CSIC-UAM
Instituto de Ciencias del Cosmos, Universidad de Barcelona

Madrid, Diciembre de 2009

Resumen

En esta tesis de máster considero en profundidad un modelo de quintaesencia recientemente propuesto, capaz de explicar la aceleración de la expansión del universo. El modelo se construye mediante una generalización de la transformación conforme y logra detener el campo escalar de una forma muy sencilla. Se analiza en detalle el comportamíento en el limite cosmológico homogéneo, encontrando un cambio muy rápido entre el regímen de seguimiento de la materia y una constante cosmológica efectiva. Se acota el espacio de parámetros con datos observacionales de supernovas, oscilaciones acusticas de bariones y el desplazamiento del fondo cosmico de microondas. Las ecuaciones que gobiernan las perturbaciones lineales son posteriormente derivadas y se explora la dinámica asociada a ellas, mostrando que el modelo es capaz de reproducir una constante cosmologica también a nivel perturbativo.

Abstract

In this master thesis I consider in depth a recently proposed type of quintessence to account for the accelerated expansion of the universe. The model is constructed by considering a generalisation of the conformal transformation which is able to produce a late slow roll phase in a very simple way. The background behaviour is analised in detail and a very quick transition between a scaling field and an effective cosmological constant is found. Observational constraints from SNe, BAO and CMB are obtained by a MCMC exploration of the parameter space. The equations governing linear perturbations are obtained and their dynamics explored. They show that the model is very able to reproduce a cosmological constant even at the inhomogeneous level.

Contents

Chapter 1

Introduction

The acceleration of the expansion rate of the universe is probably the most striking finding in cosmology since the discovery of the expansion itself. Since the first high redshift supernovae observations in the late nineties, a great amount of observational data from a number of independent sources has provided confirmation of the acceleration which is now established as a solid fact.

It can be claimed that the discovery of the acceleration might be even more striking than the discovery of the expansion itself which is a very natural consequence of the theory of General Relativity. The only simple way to achieve a static universe is the introduction of a cosmological constant tuned with infinite precision to set the universe on top of an unstable potential. This is the no-solution to the no-problem that led Einstein introduce Λ in the first place.

One decade ago, nothing was expected to depart from the attractive nature of gravity except (perhaps) a small cosmological constant. This kind of term be introduced very simply, as it is equivalent to the vacuum energy from any classical field theory. The puzzle comes with the quantum, since corrections $10^{60} - 10^{120}$ times higher than the observed value are expected to occur. Although such a *small* cosmological constant is possible, it seems extremely unnatural on the grounds of our knowledge of quantum field theory. To make things worse the fact that its density *today* is comparable to that of matter reveals yet another bizarre feature of Λ.

It seems that the same cosmological constant invoked by Einstein to make the universe unnaturally static can be used to explain the accelerated expansion that we are observing in a rather unnatural way. The true mechanism of acceleration does not need to seem natural or aesthetically pleasant to us, thus the cosmological constant is perfectly valid. However, Λ is a very simple model allowing very concrete predictions. If Λ is *not* the final answer to the acceleration of the universe evidence will be discovered sooner or later.

Triggered by this observations hundreds of models trying to explain the accelerated expansion of the universe have been proposed and investigated. Besides ideas trying

to explain the tiny value of Λ, there are numerous *dark energy* models based on modification of gravity, exotic (or even electromagnetic!) fields, extra dimensions or large inhomogeneities. Actual astronomical data do not provide very tight constraints, but it is expected that the new generation of experiments will help to put tighter bounds on these models. In the next years many of them will be ruled out whereas some of them might receive observational support. Hopefully, new surprises, findings and mysteries which we can barely imagine will be found on the way.

In this work one model of dark energy is investigated, namely *Disformal quintessence*. It is a recently proposed model based on a scalar field with a novel mechanism to trigger the acceleration which has been inspired by a generalisation of the conformal transformation present in some theories of modified gravity.

Outline

A sketch of the actual cosmological paradigm is presented in the second chapter describing its theoretical foundations, shortcomings and the observational evidence that supports it. In chapter three some aspects of scalar field models of dark energy relevant to our study are introduced.

Chapter four presents the model under study, its motivation and possible connections with already existing proposals followed by the analysis of the behaviour of the disformal field in the homogeneous limit emphasising the role of the parameters and the details of transition mechanism. Chapter five deals with the parameter constraints from supernovae, baryon acoustic oscillations and CMB shift by means of a MCMC study. The equations relevant to linear perturbation theory are outlined and the behaviour of the perturbations as well as possible observational signatures of the disformal field are addressed.

Bearing in mind that this work represents the current status of a research which is still far from complete chapter seven draws some conclusions together with the main lines of development that are being currently pursued and possible extensions of the model to be considered in the future.

Acknowledgments

This work has required a considerable amount of work and would have not been possible without the help, support and patience of many people to which I would like to express my gratitude here.

First of all, I would like to thank Tomi Koivisto. Without his careful explanations, the pacient review of my results and the long discussions we held in Heidelberg and Utrecht (often lasting until midnight) none of these pages would have been possible.

I would like to thank my advisors, Pilar Ruiz-Lapuente and David Mota for their invaluable help in providing advice and answering the great number of questions that arose during this research. I am also very thankful to my advisor within the UAM, Juan Garcia-Bellido, not only his support and advice over the years, but also for awaking my interest for cosmology in the first place during his inspiring lectures at the UAM.

Much of the work performed relied on the use and modification of the CMBEasy code. I was lucky to be able to always count on the help of one of its creators, Georg Robbers, who quickly and precisely answered all my (usually naïve) questions. I would also like to mention the help obtained from Werner Wetzel for kindly and patiently explained me the computational environment in which the MCMC run and Ramon Canal for his gentle help with the IDL plots which unfortunately I did not manage to get on time.

Further, I would like to thank Arkadi Levanyuk and Andres Cano, who besides from arising my curiosity for physics brought me the spirit of critical thinking during their unforgettable lectures in mathematical methods. Many other people need to be thanked for the great moments and interesting conversations I had with them, both within and beyond science. I would like to mention (at least) Pablo S., Edoardo Carlesi, Jose Roberto, Bryan, Dani G., Jaime, Santi, Frutos, Pablo M., Buti, Marcos, Ana (the two), Rogüa, Fer, Javi R., Tim S., Norbert and my former flatmates Emilio, Javi, Hector, Diana, Peri, Arturo and Gon. I still feel I should mention many more, but if I tried to include all and sketch how they have contributed to my life, there would be little room left for the thesis itself.

Finally and very specially, I would like to thank my parents for their invaluable support and comprehension during all these years as well as my family in Barcelona for their hospitality and generosity during my visits and always. My sister Ana, for the great moments and conversations, advice and patience, deserves a very warm mention here. And last, but by no means least, I would like to thank my dear Ania, for solving my doubts with English and very specially for keeping me smiling, even when everything seemed to be nonsense.

Miguel

Chapter 2

The Dark Energy Paradigm

We will start with a brief review of the basic properties of the standard homogeneous cosmological model that will serve us to set the notation and some fundamental equations for the rest of this work. Then, the cosmological constant problem will be stated and the astronomical support for the existence of cosmic acceleration will be then briefly discussed.

This is by no means a complete introduction in the subject, and many fundamental aspects, mostly regarding the early universe, will not be even mentioned. Good additional references can be found in [1], [2].

2.1 The Homogeneous Universe

The theory of General Relativity (GR) provides a very elegant framework in which the gravitational interactions can be related to the geometry of the spacetime [3]. It treats the geometry, represented by the metric $g_{\mu\nu}$, as a dynamical variable and associates the dynamics of the matter within it to the curvature of the space-time.

In order to determine the dynamics, an action for the metric has to be provided. It turns out that the simplest, nontrivial, well behaved theory that can be constructed for $g_{\mu\nu}(x)$ happens to explain very well all observed gravitational phenomena. It is given by the Einstein-Hilbert action

$$S = S_{GR} + S_m = \int d^4x\sqrt{-g}\frac{R}{16\pi G} + S_m\,, \tag{2.1}$$

where g is the determinant of the metric, R is the Ricci scalar and an action for the matter has been included. Variation w.r.t. the metric degrees of freedom leads to Einstein equations

$$R_{\mu\nu} - \frac{R}{2}g_{\mu\nu} = 8\pi G T_{\mu\nu}\,. \tag{2.2}$$

The left hand side of (2.2) is usually known as the Einstein tensor $G_{\mu\nu}$. The source term, the *energy momentum* tensor represents the reaction of spacetime to the matter within. It is generally defined as

$$T_{\mu\nu} = -2\frac{\delta S_m}{\delta g^{\mu\nu}} \,. \tag{2.3}$$

2.1.1 The FRW metric

GR provides a very natural description of the universe on very large scales, where gravity is the dominant interaction. In general, it is very difficult to deal with (2.2), since it consists of ten coupled, nonlinear partial differential equations. However, it is possible to construct models where the existence of symmetries greatly simplifies the equations equations.

A particularly useful choice of the metric follows the application of the *Copernican Principle* (or cosmological principle), i.e. that the universe is homogeneous and isotropic on very large scales [1]. This hypothesis is well supported by astronomical observations, as will be seen in the next section. If this symmetries are imposed on the spatial hypersurfaces, while letting their relative size evolve in time, we are led to the Friedmann-Robertson-Walker metric

$$ds^2 = -dt^2 + a(t)^2 \gamma_{ij} dx^i dx^j \,. \tag{2.4}$$

Here the *scale factor* $a(t)$ represents the overall scale of the universe at a given time. The spatial part of the metric can be written in spherical polar coordinates as

$$\gamma_{ij} dx^i dx^j = \frac{dr^2}{1 - Kr^2} + r^2(d\theta^2 + \sin^2\theta d\phi^2) \,, \tag{2.5}$$

where K parameterises the spatial curvature of the model. During most of this work we will assume that the universe as spatially flat, with $\gamma_{ij} = \delta^i_j$ and $K = 0$, as is suggested by cosmological observations. In that case, we can further redefine our coordinates to normalise the scale factor to one at present time.

The Energy Momentum Tensor

In order to model the matter content existing in a homogeneous universe, one considers the different components as perfect fluids, characterised by an energy-momentum tensor of the form

$$T_{\mu\nu} = -g_{\mu\nu}(\rho + p) + p u^\mu u^\nu \,. \tag{2.6}$$

[1] Inhomogeneities and anisotropies can be introduced as small perturbations, an approximation which makes the model much more realistic and has a wide range of applicability. In chapter 6, we will deal with the cosmological perturbations in the context of Disformal Quintessence.

u^μ is the four velocity and ρ, p the energy and pressure densities respectively. In the FRW frame, where the fluid is at rest, the four velocity is $(1, \vec{0})$) and $T^\mu{}_\nu = \mathrm{diag}(\rho, p, p, p)$.

The Friedmann Equations

One can then write down the Einstein equations for the homogeneous universe by computing $G_{\mu\nu}$ from the metric (2.4) and using (2.6) as source term. There are two independent equations, known as the *Friedmann equations*:

$$\left(\frac{\dot{a}}{a}\right)^2 + \frac{K}{a^2} = \frac{8\pi G}{3}\rho\,, \tag{2.7}$$

$$\frac{\ddot{a}}{a} = -\frac{4\pi G}{3}\left(\rho + 3p\right) + \frac{K}{a^2}\,. \tag{2.8}$$

It is conventional to define the *Hubble factor* as $H = \dot{a}/a$ and the fraction of a cosmic component as

$$\Omega_i = \frac{\rho_i}{\rho_0} \tag{2.9}$$

with $\rho_0 = \frac{3H_0^2}{8\pi G}$ the critical density needed to account for the expansion rate at present time. Note that the condition $K = 0$ is equivalent to $\rho = \rho_0$.

Cosmic and Conformal Time: Horizons

In order to write the above equations we have used *cosmic time* t as our variable. An alternative choice is the *conformal time* τ, defined through:

$$\tau = \int_0^t \frac{dt'}{a(t')}\,. \tag{2.10}$$

In terms of this coordinate the metric (2.4) reads

$$ds^2 = a(\tau)^2\left[-d\tau^2 + \gamma_{ij}dx^i dx^j\right]\,. \tag{2.11}$$

We will use both time variables in this work. To distinguish them, we will always denote cosmic time derivatives with a dot ($\dot{f} = df/dt$) and conformal time derivatives with a prime ($f' = df/d\tau$). Both derivatives are easily related by differentiating (2.10)

$$\dot{f} = \frac{f'}{a} \quad \text{and} \quad \ddot{f} = \frac{1}{a^2}(f'' - \mathcal{H}f')\,. \tag{2.12}$$

The *conformal Hubble factor* above has been defined as $\mathcal{H} = a'/a$.

One very important feature of the conformal time is that it is equivalent to the *comoving horizon* at a given time, i.e. the coordinate distance that a light signal has

been able to travel since the first instants of the universe. As this measures scale at which causal physics has had time to occur, it is a very important in the analysis of perturbations in a relativistic theory. For example, two points of the universe can not feel mutual gravitational attraction before they enter in the horizon of each other.

2.1.2 The Standard Cosmological Model

From the conservation equation for the energy momentum tensor $\nabla_\mu T^{\mu 0} = 0$ the *continuity equation* is obtained:

$$\dot{\rho} + 3H(\rho + p) = 0\,. \tag{2.13}$$

For most of the cosmic evolution, the dominant fluids can be treated as *barotropic*, for which $p = w\rho$. It follows that for a constant equation of state:

$$\rho \propto a^{-3(1-w)}\,. \tag{2.14}$$

Most cosmic fluids fit well in this description: Radiation and cold matter both have constant w with values 0 and 1/3. Matter scales as a^{-3} because it gets diluted, the number of particles remaining constant. Radiation, on the other hand scales as a^{-4}. This difference happens because photons gets diluted and *redshifted*, loosing energy individually as their wavelength are stretched by the expansion of the universe. This provides a very convenient cosmological variable to use instead of the rather unphysical comoving coordinates $\vec{x}$. The Redshift from light emitted when the scale factor was a_* is

$$z = \frac{1}{a_*} - 1\,. \tag{2.15}$$

Another interesting fluid is the cosmological constant. It can be introduced by substituting $R \to R - 2\Lambda$ in 2.2, leading to an action piece

$$S_\Lambda = \int d^4x\sqrt{-g}\frac{\Lambda}{8\pi G}\,. \tag{2.16}$$

It is equivalent to a fluid with $T_{\mu\nu} \propto g_{\mu\nu}$, for which with $p = -\rho$. Then the scaling relation becomes $\rho_\Lambda =$ constant representing a constant vacuum energy independent from the expansion.

The Components of the Universe

In addition to General Relativity, the assumptions of homogeneity and isotropy and the statistical physics that describes the hot plasma present at early times [2], the Standard

[2] A more realistic description of the universe requires the specification of initial conditions for the perturbation. The paradigm of *cosmic inflation*, an stage of accelerated expansion at early times, provides concrete predictions for this initial perturbations and is normally considered part of the standard cosmological mode, if well the specific mechanism of this expansion is unknown. In addition, inflation is able to solve several fine-tuning problems of standard cosmology. See for example [4]

Cosmological Model assumes the following ingredients:

- (No) Curvature: Despite it is not a component in itself, it can be quantised in terms of $\Omega_k = 1 - \Omega = \frac{K}{\rho_0 a^2}$. Observations of the peaks of the CMB anisotropies are compatible with little or no curvature at all.

- Baryons: The term is used generically for electromagnetic interacting particles. It is known from the primordial deuterium abundance that they account for approximately $\Omega_b = 0.05$ of the total energy density.

- Photons: The CMB is the best blackbody observed ever. Its temperature $T = 2.725K$ was measured by the COBE satelite, from which we can infer the value $\Omega_\gamma = 4.7 \cdot 10^{-5}$.

- Neutrinos: Despite not being directly observed, the amount of cosmological neutrinos can be calculated within the hot Big Bang theory to be $\Omega_\gamma = 3.2 \cdot 10^{-5}$. Properties such as their mass or the number of species do have cosmological implications and can be constraint from observations.

- Cold Dark Matter: To correctly explain the formation of structure, there must be a significant amount ($\Omega_{CDM} \approx 0.23$) of nonrelativistic, non electromagnetically interacting matter. Other astrophysical observations, such as rotational curves of galaxies or gravitational lensing strongly support their existence.

- Cosmological Constant: The most economic description for the accelerated expansion and the flatness of the universe is a cosmological constant or vacuum energy with $\Omega_\Lambda \sim 0.7$.

Since the first four points in the above list are rather well established, the aforementioned model is usually denoted ΛCDM (Lambda-Cold-Dark-Matter). There is little controversy about the existence of Dark Matter as an unknown particle species. Many experiments for its detection or direct production are actually being performed to distinguish among the wealth of models[3]. In principle, any given particle physics model makes definite predictions regarding the relative abundance today and signals expected in astronomy and particle detectors. In this sense, the problem is very well posed and it seems that only more accurate data is needed to determine what is out there.

2.1.3 The Cosmological Constant Problem

On the other hand, there seems little to be done for the case of Λ: It is a constant in space and time, with an equation of state equal to -1. It does not cluster or interact

[3]These include ground based detectors, astrophysical observations of their possible annihilation and of course the LHC. Actually, there are several recent claims of DM detection.

with any other species, and seems extremely difficult or impossible to detect in a laboratory or by means of local gravity tests. If it is the final answer, all cosmologists can do is to constraint it's value.

If this is the case there are two aesthetically unpleasant issues to be dealt with. The first one (the original cosmological constant problem) is related to the fact that the contributions to the vacuum energy expected from particle physics are huge in comparison to the observed value. If quantum field theory is regarded as an effective theory, valid up to a certain energy scale Λ_{cutoff}, then the naive contribution to the vacuum energy is of order Λ^4_{cutoff}. The failure to obtain a quantum field theory of gravity, for which the scale is the Planck Mass $M_p = 2.43 \cdot 10^{18} GeV^4$ points towards $\Lambda_{cutoff} = M_p$. It is no theoretical problem to renormalise this huge vacuum energy, but the cancellation happens to occur to a precission of one part in 10^{120}, which seems very unnatural [5].

The second problem is of cosmological origin, and is called the *coincidence problem*. The energy densities of matter and radiation are similar today, but their relative scaling ($\rho_\Lambda/\rho_m \propto a^3$) implies that the fraction of cosmological constant was completely negligible in the cosmological past and will be absolutely dominant in the future. For example, when the first stars formed in the reionization epoch, $z \sim 11$, dark energy was completely negligible $\rho_\Lambda/\rho_m \propto 10^{-3}$. Then the question arises, how likely it is to be observing this special moment?

Alternatives to Λ

In an effort to provide phenomenologically richer and theoretically more pleasant alternatives to Λ, a vast amount of proposals have been considered [6], [7]. These alternatives usually appeal to an unknown principle to set the vacuum energy to zero (for example, a fundamental symmetry of consistency requirement of quantum gravity) and provide an alternative mechanism to accelerate the universe. Some directions include:

- Dropping the Copernican principle. One possibility is consider large inhomogeneities, the acceleration would be only apparent if we were living close to the centre of a big underdensity [8]. It has also been suggested that the acceleration might be produced by not properly taking into account the nonlinearity of Einstein equations in the Copernican average.

- Adding new exotic matter: In principle, a new kind of cosmological fluid could be producing the acceleration. An scalar field can achieve a negative equation of state if it moves slow, and actually most inflationary models make use of them to provide early time acceleration.

[4]By M_p we will refer to the reduced Planck mass $M_p = (8\pi G)^{-1/2}$.

- Dropping General Relativity. It could be possible that Einstein theory is not valid on the large scales explored by cosmology and has to be modified in the far infrared. Possibilities include the addition of more terms to (2.1), couple scalars to curvature invariants or include extra dimensions (as is suggested by string theory).

2.2 Observational Evidence

Two complementary sets of evidence point towards the existence of dark energy. First, distant supernovae appear fainter as they would be in a matter dominated universe, probing the acceleration directly. Second, precise measurements of CMB anisotropies indicate that our universe has very small or no curvature. The study of the matter power spectrum constraints the amount of ordinary matter to be about one third of the critical density, indicating the presence of an additional energy component.

2.2.1 Distant Supernovae

The first direct evidence from the current acceleration of the universe came from the observation of the luminosity distance curve from extragalactic type 1A Supernovae [9, 10]. These objects are extremely intense explosions that occur when the mass of a white dwarf accreting matter from a companion star reaches the Chandrasekhar mass ($\sim 1.43 M_\odot$). After this point is reached electron degeneracy pressure is not able to mantain the size of the star, leading its collapse and explosion as the nucleon degeneracy pressure is reached.

It is believed that this process gives rise to phenomena with the same intrinsic luminosity regardles of the composition of the original star. However, individual differences are observed among the SNe Ia, which can fortunatelly be corrected by other observed properties [11]. After correction, the distance modulus reads

$$\mu = m_B^{\max} - M + \alpha(s-1) - \beta c \,, \tag{2.17}$$

where $m_B^{\max}$ is the maximum observed magnitude and M the (unknown) absolute magnitude, corrected by the stretch (s) and the colour (c) of the SNe. α and β are phenomenological parameters that need to be fitted through the data.

The *luminosity distance* is defined by comparison of the observed flux $\mathcal{F}$ and the known brightness at surface

$$L_s = d_L^2 4\pi \mathcal{F} \,, \tag{2.18}$$

and it corresponds to the physical distance in a flat, static space-time. It is related to the distance modulus by

$$\mu = 5 \log(H_0 d_L(z)) \,. \tag{2.19}$$

d_L can be calculated in terms of cosmological variables by taking into account the expansion of the universe and the luminosity loss due to photon delay and redshift. For a flat universe:

$$d_L = (1+z)\int_0^z \frac{dz'}{H(z')}\,. \tag{2.20}$$

Equation 2.20 is sensitive to the expansion rate of the universe and its evolution at late times, when H is lower. Plotting the measured values for different SNe provides valuable information on the amount of dark energy and its equation of state as a function of redshift.

Since the absolute luminosity of SNe is not know theoretically, the data analysis relies on the comparison between nearby and distant events. The former allow the determination of M, which can be then compared with the high z objects to constraint the Hubble diagram. There are of course many identified uncertainties that have to be considered when using SNe as cosmological probes [12]. However, modern wealth of high quality data allow for a consistent study of this systematic error sources and a variety of cross checks that validate their use as standard candles [13].

2.2.2 Cosmic Microwave Background

The Cosmic Microwave Background radiation (CMB) is a thermal bath of photons, an extremely precise $2.7K$ blackbody released when the hot plasma was cool enough to form neutral hydrogen, making the universe transparent. It is the most firm evidence of the expansion of the universe and a great indicator of its isotropy on large scales. After substraction of the background value and the dipole (due to the peculiar velocity of our galaxy), CMB anisotropies are found at the level of $\delta T \sim 100\mu K$. Several experiments have measured these anisotropies in recent years, significantly improving our knowledge of the Universe.

There are two major CMB features of the CMB that can help us to constraint the properties of Dark Energy.

Position of the Acoustic Peaks

The Universe at temperatures above few eV contained a plasma in which photons and baryons were tightly coupled due to Thomson scattering processes. Sound waves excited by the primordial perturbations were able to propagate in this plasma with a velocity $c_s \approx 1/\sqrt{3}$. At $z_* \approx 1080$, the expansion of the Universe reduces the temperature enough to alow the formation of stable hydrogen (*recombination*), releasing the photons and freezing the sound waves.

The radiation we see reflects this pattern of acoustic waves as it was imprinted at recombination. The comoving length the sound waves had been able to travel since

the earliest times determines which Fourier modes correspond to maxima and minima through the condition:

$$k \int_0^{t_*} \frac{c_s}{a} dt = \frac{n\pi}{2} \tag{2.21}$$

The integral in the above expression known as the comoving sound horizon at recombination (r_s). It can be known given the amount of matter and baryons, since they influence the sound speed c_s. As its value is known, it can be used as a *standard ruler* by comparing its size at high redshift with its size today. One defines the angular diameter distance d_A via

$$\theta = \frac{r}{d_A} = \frac{r(1+z)}{\int_0^z \frac{dz'}{H(z')}} \ , \tag{2.22}$$

where r is the size of the standard ruler at redshift z, θ is the angle it subtends in the sky today. The second equality is the value for a flat FRW metric. The dependence on the cosmological parameters is given by the Hubble factor in the integral, and therefore the angle subtended by the acoustic scale will depend on the cosmological parameters. This provides an stringent test for the flatness of the universe and helps to constraint the properties of dark energy.

Integrated Sachs Wolfe Effect

Other effect of interest occurs in the lowest multipoles of the CMB, corresponding to the largest scales available to observation [14]. As it was mentioned in section 2.1.1 each Fourier mode begins to grow by gravitational instability only when its physical size becomes similar to the horizon, i.e. $\tau k \approx 1$. This means that the low l anisotropies are seen as they were created in the very early universe (see footnote 2 in this chapter), only affected by the last stages of the cosmic evolution.

Photons on their way from the surface of last scattering will be blue and redshifted as they fall into or escape from gravitational wells. If their depth remains constant, as is the case in a matter dominated Universe, the energy gained by the photon as it enters the overdensity will be compensated by the loss from climbing out, and the effect averages out statistically.

Deviations from matter domination have an impact on this large scales. A faster expansion tends to wash out the potentials, therefore producing a net temperature gain on the corresponding large angular scales, which is a complementary probe of the acceleration. Other effects might become manifest through the ISW effect in models beyond Λ due to their different clustering properties.

2.2.3 Large Scale Structure

As successful as it is in the description of the CMB anisotropies, cosmological perturbation theory can also explain how matter clustered by means of gravitational attraction

and gave birth to the cosmic structure we observe today. It is based on the approximation that the matter overdensity is small $\delta = \rho(\vec{x})/\rho \ll 1$. Even being wildly broken on small scales, such as galaxies, perturbation theory is an excellent approximation to the physics corresponding to large scales. Nonlinear evolution becomes important for $k < 0.1hMpc^{-1}$ at present times, and in earlier times, nonlinear effects were significant only on increasingly smaller scales.

In order to get ordinary differential equations, perturbations are studied in Fourier space. The smallness of the perturbations ensures that each $k-$mode evolves independently and once initial conditions are provided, the evolution of each mode can be calculated for the different particle species. There is a rich phenomenology associated with the growth of cosmic perturbations. For example, the growth of modes entering at early times is very strongly suppressed by the pressure produced by hot relativistic matter. These wavelengths start evolving significantly only after the equality time, which is the cause of the turnover observed in the CDM power spectrum.

This feature allows the observational determination of the equality scale, linked with the total amount of matter $\Omega_m \approx 0.3$. Together with the constraints on Ω_k from the CMB discussed above, the presence of an additional energy component can be inferred independently from SNe observations.

Baryon Acoustic Oscillations

The matter power spectrum also reflects the oscillations occurred in the baryon-photon fluid before recombination. In $k-$space, these correspond to a wiggle on the power spectrum.Contrary to the CMB, these oscillations are difficult to detect in the matter spectrum because they are surpressed by the small fraction of baryons compared to CDM.

To get a cartoon picture of how the baryon acoustic oscillations form, consider a primordial perturbation in the baryon and CDM density located at the origin. This produces a sound wave that travels in the baryon-photon fluid with the speed of sound. At recombination, the propagation finishes, and the sound wave freezes as a spherical overdensity at a distance corresponding to the sound horizon at recombination ($r_s(\tau_*)$) away from the initial perturbation. When this effect is considered for more realistic initial conditions, i.e. a superposition of primordial overdensities, the BAOs are reflected as a slight bump in the two point correlation function of galaxies, as was first reported in 2005 [15].

As we mentioned, the acoustic scale is a standard ruler that is observed with a certain angular scale in the CMB spectrum. Measuring the BAO scale at different redshifts allows for a complementary probe of the Hubble diagram. In principle, two acoustic scales can be measured at any redshift:

- The transverse BAO scale, orthogonal to the line of sight. It can be related to

the Hubble diagram by means of an angular diameter distance, which is related to H through an integral in redshift.

- The radial BAO scale, parallel to the line of sight. Its evolution is directly related with the Hubble factor at a given redshift, and its measurement would constitute the most direct exploration of the dynamics of dark energy.

Actual galaxy surveys are not able to distinguish the angular and radial acoustic scales. Current methods measure a certain combination of both scales, as is briefly explained in section 5.1.2. Sufficiently precise galaxy surveys should be able to distinguish both at different redshifts, yielding a very accurate description of the acceleration of the universe and possible dynamics of dark energy.

Chapter 3

Scalar Dark Energy

We will briefly review some general aspects of scalar dark energy that are relevant to our model. As we will see in chapter 4 we will be dealing with a generalised quintessence (K-essence) field that behaves as normal quintessence early in the cosmic history, mimicking the behaviour of the dominant fluids. The non-standard features become relevant at late times, when the field drives the accelerated expansion.

3.1 Quintessence

A very simple way to achieve an accelerated expansion is by the introduction of a scalar field. This scenario has been very well explored in the construction of inflationary models, and more recently to provide dynamical alternatives to the cosmological constant, if well there was some activity in the field before the discovery of the accelerated expansion [16, 17]. In addition, scalar fields with certain potentials are able to "follow" the dominant component during most of the cosmic evolution, thus helping to solve the coincidence problem.

The term quintessence denotes a scalar field ϕ, with a canonical kinetic term and a potential which is minimally coupled to gravity and produces a late phase of accelerated expansion. It is described by the action:

$$S_q = \int d^4x\sqrt{-g}\left[-\frac{1}{2}g^{\mu\nu}\partial_\mu\phi\partial_\nu\phi - V(\phi)\right] . \tag{3.1}$$

Variation with respect to the inverse metric and the scalar field lead to the energy-density tensor and the Klein-Gordon equation:

$$T^{(q)}_{\mu\nu} = \partial_\mu\phi\partial_\nu\phi - g_{\mu\nu}[\frac{g^{\alpha\beta}}{2}\partial_\alpha\phi\partial_\beta\phi + V(\phi)] , \tag{3.2}$$

$$\nabla_\mu\nabla^\mu\phi - V_{,\phi} = 0 . \tag{3.3}$$

For the FRW background cosmology, the above expressions reduce to

$$\rho_q = \tfrac{1}{2}\dot{\phi}^2 + V(\phi) \quad , \tag{3.4}$$

$$p_q = \tfrac{1}{2}\dot{\phi}^2 - V(\phi) \quad , \tag{3.5}$$

$$\ddot{\phi} + 3H\dot{\phi} + V_\phi = 0\,. \tag{3.6}$$

We can obtain the equation of state for a scalar field as

$$w_q = \frac{\frac{1}{2}\dot{\phi}^2 - V}{\frac{1}{2}\dot{\phi}^2 + V}\,. \tag{3.7}$$

(3.7) shows that a scalar field can achieve a negative equation of state if $\frac{1}{2}\dot{\phi}^2 < V(\phi)$ (i.e. if the field is *slow rolling*) and possibly accelerate the cosmic expansion.

3.1.1 Scaling Behaviour

Let us briefly discuss under which conditions a quintessence field can mimic the energy density of a dominant barotropic fluid[1]. This property does not only help to alleviate the coincidence problem, it also allows us to do without specifying the initial conditions for the field, since most natural initial conditions will reach the attractor before any epoch of interest [19].

For exponential potentials (among others), it is found that for most initial values of the field, a *scaling solutions* is achieved in which the fraction of dark energy remains constant. The necessary idea to reach this result is to regard the Friedmann equations (2.7), (2.8) and the Klein-Gordon equation (3.6) as a dynamical system and study the phase space to search for stable solutions [20].

Stability of Fixed Points

An autonomous system is a set of ordinary differential equations with no explicit time dependence ($\partial_t f = 0$):

$$\frac{d}{dt}\xi^i(t) = \; f^i(\{\xi^j(t)\}) \tag{3.8}$$

Fixed points $\vec{\xi}_0$ occur whenever $\dot{\vec{\xi}}_0 = \vec{f}(\vec{\xi}_0) = 0$. One can then study whether these points are stable, i.e. if a solution close to the point will remain close. In that case the fixed point is called an *attractor*. More precisely, one asks if $|\vec{\xi}_0 + \vec{\delta}(t)|$ is bounded. An expansion of 3.8 around the fixed point yields a linear system

$$\frac{d}{dt}\delta^i = \frac{\partial f^i}{\partial \delta_k}\delta^k + \mathcal{O}(\delta^2) \tag{3.9}$$

[1]For a similar discussion in the context of k-essence, see [18]. We will however restrict ourselves to usual quintessence since the disformal field is indistinguishable from it at the tracking stage.

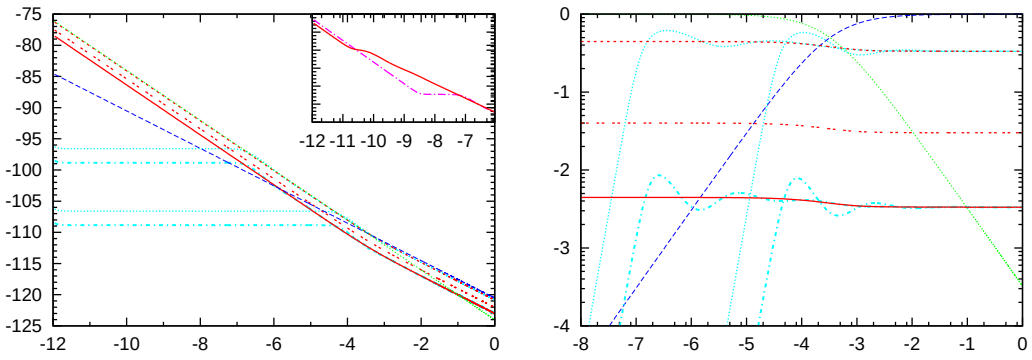

Figure 3.1: Tracking Behaviour for exponential quintessence: $\log(\rho)$ in units of Mpc^{-4} (left) and $\log(\Omega)$ (right) as a function of $\log(a)$. Green and dark blue lines are radiation and matter respectively. The red lines correspond to exponential quintessence with α values of 3 (dotted), 10 (double dotted) and 30 (straight). The light blue lines correspond to fine tuned initial energy density, with values 10^{-20} and 10^{-30} times the value at the attractor ($\alpha = 30, 3$ in the dash dotted and dotted lines respectively). Note how they are "captured" by the attractor solution when they reach it. The detailed view of the left plot shows how a solution with $\rho_0 = 10\rho_0^{\rm att}$ is attracted at initial times. Solutions with much larger initial dark energy density than radiation density will also fall in the attractor or in the fine tuned solutions, since their dilution is very effective when they dominate the energy budget. All displayed initial conditions assume equal kinetic and potential energy.

It is then possible to diagonalise the matrix $\hat{M} = \partial f/\partial\delta$. For the basis eigenstates $\hat{M}\vec{\mu}_\alpha = \lambda_\alpha\vec{\mu}_\alpha$ the linear system decouples and the solutions are

$$\mu_\alpha(t) = \mu_\alpha^{(0)} e^{\lambda_\alpha t} \tag{3.10}$$

Clearly, a negative eigenvalue indicates the presence of an unstable direction along which the trajectory is likely to leave the fixed point. Then $\Re(\lambda_\alpha) > 0, \forall\alpha$ is required in order to have an attractor[2].

[2] A general matrix will have both real and complex eigenvalues, where the second occur in complex conjugate parts. For a conjugate pair of eigenvalues $\lambda_\pm = \vartheta \pm i\omega$, the imaginary part will produce an oscillation between the coordinates μ_+ and μ_-. The real part will be associated with a damping if $\vartheta < 0$ or an instability if $\vartheta > 0$. The fixed point is called a *stable spiral* in the first case.

Existence of Scaling Solutions

In this section we will suppose that the potential is an exponential function $V = \exp(-\alpha\phi/M_p)$. Defining the variables

$$x = \frac{\dot{\phi}}{4\sqrt{3\pi G}H}, \quad y = \frac{\sqrt{V}}{2\sqrt{6\pi G}H}, \quad N = \ln(a) \tag{3.11}$$

one can rewrite the system of equations given by (2.7), (2.8) and (3.6) as [20]:

$$\frac{d}{dN}x = -3x + \frac{\sqrt{6}}{2}\alpha y^2 + \frac{3}{2}x[(1-w_m)x^2 + (1+w_m)(1-y^2)] \tag{3.12}$$

$$\frac{d}{dN}y = -\frac{\sqrt{6}}{2}\alpha xy + \frac{3}{2}y[(1-w_m)x^2 + (1+w_m)(1-y^2)] \tag{3.13}$$

where w_m is the state equation for the matter/radiation fluid and is assumed to be constant. The Friedmann equation is then:

$$x^2 + y^2 + \frac{8\pi G\rho_m}{3H^2} = 1 \tag{3.14}$$

We can read the dark energy fraction and equation of state from (3.11)

$$\Omega_q = x^2 + y^2, \quad w_q = \frac{x^2 - y^2}{x^2 + y^2} \tag{3.15}$$

Analysis of the fixed points in (3.12) and (3.13) yields the following stable fixed points [20]:

	Ω_q	$1 + w_q$	Existence
a)	1	$1 - \alpha^2/3$	$\alpha^2 < 3(1 + w_m)$
b)	$3(1 + w_m)/\alpha^2$	w_m	$\alpha^2 > 3(1 + w_m)$

we see that a) corresponds to an Universe dominated by dark energy at early times, which is not interesting for our purposes. However, in b) the field mimics the behaviour of the dominant matter, with constant ρ_ϕ/ρ_m (*tracking behaviour*). This solution is generically reached by the field, unless its initial energy fraction is extremely large or small. Figure 3.1 illustrates the tracking behaviour of the field for different parameters and initial conditions.

The possibility of tracking can alleviate the coincidence problem, since now the proportion of early dark energy is the same during most of the cosmic evolution. It only remains the question of how can the field be tossed out of the attractor, which is impossible in the case of the pure exponential potential studied above.

Transition Mechanisms

At some point, the scaling era has to end in order to obtain an accelerated expansion. Several possibilities have been considered to toss the field out of the attractor

- Introducing a suitable bump into the form potential [21].
- Taking into account the Gauss-Bonnet term [22, 23].
- Coupling the field to other matter [24, 25].
- Introducing many fields [26].
- Considering noncanonical Lagrangian. This possibility leads naturally to the (generalised) k-essence scenario. Since we can encompass disformal quintessence in this category, we will briefly discuss it in the next section.

3.2 (Generalised) K-essence

The term k-essence stands for kinetically driven quintessence and was introduced by [27], [28] where a noncanonical kinetic term was responsible for the accelerated expansion. In its most general formulation consists of a generalisation of the action 3.16[3]:

$$S_k = \int d^4x \; p(X, \phi) \,, \tag{3.16}$$

Where

$$X \equiv \frac{1}{2}\phi^{,\alpha}\phi_{,\alpha} \,. \tag{3.17}$$

Any scalar field models minimally coupled to gravity can be described by 3.16, and it has been shown that inconsistencies are expected to occur in many cases, such as superluminal motion [29] or classical and quantum instabilities [30].

The energy momentum tensor for the action (3.16) can be obtained through equation 2.3 by noting that the only metric dependence in p occurs via X. Since $\delta\sqrt{-g} = -\sqrt{-g}g_{\mu\nu}\delta g^{\mu\nu}$, direct differentiation yields

$$T^{(p)}_{\mu\nu} = \frac{2}{\sqrt{-g}}\frac{\delta p}{\delta g^{\mu\nu}} = p(X,\phi)g_{\mu\nu} - p_{,X}(X,\phi)\phi_{,\mu}\phi_{,\nu} \,, \tag{3.18}$$

from which we can read the values of the energy and pressure density in the flat FRW background:

$$\rho = T_{00} = -p - p_{,X}\dot{\phi}^2 \,, \tag{3.19}$$

$$p = T_{ii} = p \,. \tag{3.20}$$

[3]In the literature, the term k-essence usually refers to models with $p = f(X)g(\phi)$.

This is the reason to denote the Lagrangian density by p: It is equal to the pressure in the FRW frame. Note that both quantities in (3.20) are in principle different. The Lagrangian density (l.h.s.) and is a scalar, invariant under general coordinate changes. The pressure at the r.h.s. is a three scalar, invariant only under spatial rotations. However, since we will only refer to the pressure in the FRW frame, we will not distinguish them in the equations. The generalisation of the Klein-Gordon equation can be obtained by direct variation with respect to ϕ:

$$\nabla_\mu(p_{,X}\partial^\mu\phi) - p_{,\phi} = 0\,. \tag{3.21}$$

Expanding the covariant derivative for the FRW case yields

$$[p_{,X} - p_{,XX}\dot{\phi}^2]\ddot{\phi} + 3Hp_{,X}\dot{\phi} + p_{,\phi} + p_{,X\phi}\dot{\phi}^2 = 0\,. \tag{3.22}$$

Chapter 4

Disformal Quintessence

4.1 Disformal Transformations

The model under study [31] consist of a scalar field living in a barred metric $\bar{g}_{\mu\nu}$, related to the physical one by means of a *disformal transformation*:

$$\bar{g}_{\mu\nu} = A(\phi)g_{\mu\nu} + B(\phi)\partial_\mu\phi\partial_\nu\phi \tag{4.1}$$

The special case $B = 0$ is to a conformal transformation, very well known from gravitational physics and cosmology [32]. Many alternatives to GR in which the gravitational part of the action is modified can be reduced to a Einstein-Hilbert action form by means of a conformal transformation, as in the case of scalar tensor and $f(R)$ theories. In this cases, the metric in which the original theory is formulated is said to be given in the *Jordan Frame*, while the metric for which the gravitational part reduces to the Einstein-Hilbert form is said to be in the *Einstein Frame*. This simplification of the gravitational sector is transferred to the matter sector in the form of a non minimal interaction with gravity. Since conformal transformations preserve the causal structure of both geometries, they help to avoid theoretical pathologies such as superluminal motion.

In more general cases, lightcones are not preserved and the causal structure of the two spacetimes is different. It has been argued that equation 4.1 is the most general relation between two metrics that respects causality, covariance and the weak equivalence principle introducing only one scalar spacetime function [33]. Hence, if there is a physical metric in which the matter is minimally coupled, and a gravitational metric which obeys the well behaved Einstein Equations, disformal transformations are in some sense the most general relation between both.

The study of models unifying dark energy and dark matter has often encountered disformal relations. A variation of the disformal transformation has been considered in Bekenstein's TeVeS (Tensor-Vector-Scalar), the relativistic version of MOND (Modified

Newtonian Dynamics) [34]. The theory is constructed by assuming that the relation between the physical and gravitational geometries is given by a disformal transformation in which the second term is provided by a vector function instead of the gradient of the scalar. This modified gravity theory is able to explain gravitational lensing as well as rotational curves of galaxies without a dark matter component, but it fails to explain the dynamics of galaxy clusters.

Disformal transformations also allow to relate a bigravity theory, in which two metrics couple through a term $q^{\mu\nu}g_{\mu\nu}$, to an Einstein Born Infeld theory [35]. EBI theories have been shown to mimic dark matter at galactic and cosmological scales, but they can not simultaneously provide an accelerated expansion [36].

For the case of homogeneous cosmology and since we are interested in dark energy, one can obtain the relation between the physical and gravitational energy and density pressure in the disformal case as [31]:

$$\rho = \left(1 - B\dot{\phi}^2/A\right)^{-\frac{1}{2}} \bar{\rho} \tag{4.2}$$

$$p = \left(1 - B\dot{\phi}^2/A\right)^{\frac{1}{2}} \bar{p}\,. \tag{4.3}$$

With the barred values being computed with respect to the disformed metric 4.1. From the above expression it is clear that the disformal relation does not generate effective pressure for a fluid for which the pressure vanishes. Hence a pure disformal relation can not accelerate the expansion in a pure matter setting.

It turns out that the most simple model for which (4.1) becomes relevant also provides a form of dark energy. Let us consider a cosmological constant living in a disformal metric:

$$S_{\bar{\Lambda}} = \int d^4x\sqrt{-\bar{g}}\Lambda\,. \tag{4.4}$$

This action describes unstable branes in string theory [37, 38]. Its equation of state can be calculated through (4.2,4.3) to be

$$p = -\frac{\Lambda^2}{\rho},. \tag{4.5}$$

Thus the cosmological term of a disformal metric is a tachyon in a constant potential. The above equation of state is known as Chaplygin gas and has been applied in cosmology in attempts to unify dark matter and dark energy [39].

4.1.1 The Model

One is tempted to explored other possibilities arising from the disformal relation. One step further would be to apply the disformal prescription to the minimal quintessence scenario.

Metric 4.1 has an interesting property: Any kind of matter living in $\bar{g}_{\mu\nu}$ will feel little or no time flow whenever $B(\phi)\dot{\phi}^2 \sim A(\phi)g_{00}$. In the context of cosmology, this can force a scalar field to slow-roll and accelerate the expansion of the Universe[1] . We shall consider the most simple possibility, namely that the field slowing down the time flow and the one causing the acceleration are the same. Direct substitution of $g_{\mu\nu} \to \bar{g}_{\mu\nu}$ in the minimal quintessence Lagrangian (eq. 3.1) leads to the action for *disformal quintessence*:

$$S_\phi = \int d^4x\sqrt{-\bar{g}}\,[-\bar{g}^{\mu\nu}\partial_\mu\phi\partial_\nu\phi - V(\phi)]\ . \tag{4.6}$$

Action (4.6) is useful to remark the physical interpretation of the theory. On the other hand, it obscures the relation to the physical metric $g_{\mu\nu}$ and makes computations more difficult. An equivalent [31] and more convenient description is to treat the theory as a k-essence with the action given by equation 3.16 and a Lagrangian density of the form

$$p(\phi, X) = -A^{\frac{3}{2}}(\phi)\Big(\frac{X}{\sqrt{A(\phi)+2B(\phi)X}} + \sqrt{A(\phi)+2B(\phi)X}V(\phi)\Big)\,. \tag{4.7}$$

To prove the equivalence, we first relate the determinants of the two metrics as (see Appendix C of Ref.[34])

$$\sqrt{-\bar{g}} = A^2\sqrt{1+2\frac{B}{A}X}\sqrt{-g}\,. \tag{4.8}$$

This gives the potential term in p. For the kinetic term we also need the inverse metric, which we can obtain by contraction with an Ansatz $\bar{g}^{\mu\nu} = C(X,\phi)g^{\mu\nu} + D(X,\phi)\phi^{,\mu}\phi^{,\nu}$

$$\bar{g}^{\alpha\beta} = \frac{1}{A}\left(g^{\alpha\beta} - \frac{B}{A+2BX}\phi^{,\alpha}\phi^{,\beta}\right)\ . \tag{4.9}$$

Hence, the disformal kinetic term is

$$\bar{X} = \frac{X}{A+2BX}\,. \tag{4.10}$$

For the sake of simplicity, we will restrict to the purely disformal case $A = 1$. We further choose B and V to be exponential functions of the field

$$B(\phi) = \frac{B_0}{M_p^4}\ e^{\beta\phi/M_p} \tag{4.11}$$

$$V(\phi) = M_p^4\ e^{-\alpha\phi/M_p}\,. \tag{4.12}$$

This choice for V ensures a scaling stage in the early Universe and thus certain independency from the initial conditions. It seems natural to make a similar choice for B.

[1] This idea has also been considered in the context of inflation [40] with negative results.

It is further justified by the necessity of B reaching $1/V$ for the disformal features to become important. Different functional forms for the functions might achieve this condition in a rather unnatural way. No coefficient has been given to the potential since its scale is assumed to be given by the initial value of the field ($V_0 = \exp(-\alpha\phi_0/M_p)$). Similarly, we will usually consider that the scale of the disformal function will be given in terms of a field offset as $B_0 = \exp(\beta\phi_x/M_p)$.

Exponential potentials arise quite naturally in theories with extra dimensions [19, 41]. For example, in six dimensional Kaluza-Klein theories, the kinetic energy of the compactified dimension depends on the logarithmic derivative of the characteristic compactification length L. Defining a field proportional to $M_p \ln(L)$ naturally leads to an effective theory consisting in four dimensional general relativity plus a minimally coupled field with an exponential potential. Similar potentials are known to arise in higher order gravity theories, supergravity and string theoretical models.

Appendix A contains the derivatives of the Lagrangian density 4.7 which are relevant for our computations.

4.1.2 Relation to Other Models

As we have seen, the disformal relation has a very simple connection with the Chaplygin gas. It turns out that a slight generalisation of 4.7 is able to encompass a wide variety of quintessence models. If we write

$$p(\phi, X) = -\frac{\varepsilon_1 X}{\sqrt{1+\varepsilon_2 2B(\phi)X}} - \sqrt{1+\varepsilon_3 2B(\phi)X}V(\phi)\,, \tag{4.13}$$

where $\varepsilon_i = 1, 0, -1$, the different possibilities relate to many different models discussed in the literature and might suggest new interesting generalisations. Some of this relations are briefly sketched in table 4.1.

ε_1	ε_2	ε_3	Model	Remarks
0	0	0	Cosmological constant Λ	$w = -1$
1	0	0	Quintessence	$w > -1$, Eq. 3.1
-1	0	0	Phantom Quintessence	$w < -1$
0	0	1	Chaplygin Gas	$\bar{p} \propto \rho^{-1}$
1	0	1	Tachion Condensate	[42]
1	1	1	Disformal Quintessence	[31], this work
-1	1	1	Phantom Disformal Quintessence	to be continued...

Table 4.1: Some models of Dark Energy related to disformal quintessence by means of 4.13. The list is not complete, but includes some well known DE candidates, ruled out models and possible extensions to disformal quintessence.

The models where the disformed metric interpretation (equation 4.6) is valid are those with $\varepsilon_2 = \varepsilon_3 = \pm 1$. The case $\varepsilon_2 = \varepsilon_3 = -1$ would produce a phase in which the field speeds up instead of slowing down when the disformal effects become manifest, and is not likely to be interesting as dark energy. This possibility was also ruled out in [33] on the grounds of causality violation.

Another possibility is to only flip the sign of the kinetic term ($\varepsilon_3 = -1$) to obtain a phantom field. In this case, the disformal effect might be able to render the model stable at the classical level by slowing down the field at a certain point.

Finally, there is another possibility to extend the model by constructing the kinetic term with the contravariant field derivatives $\hat{X} = \frac{1}{2}\bar{g}_{\mu\nu}\phi^{,\mu}\phi^{,\nu}$. For this case, the Lagrangian density in terms of the physical metric acquires a slightly different form

$$p(\hat{X}, \phi) = -A^{\frac{3}{2}}\sqrt{A + 2BX}\,[X(1 + 2BX) + V(\phi)]\ . \tag{4.14}$$

4.2 Dynamics of the Disformal Field

In these section we will explore the phenomenology of disformal quintessence in the unperturbed FRW metric. We first expose the relevant equations and then explore the two regimes of interest:

1. At early times the disformal factor is negligible and the field behaves as normal quintessence, tracking the dominant component.

2. At some point, the disformal factor becomes of order unity, freezing time flow in $\bar{g}_{\mu\nu}$ and producing a loss of kinetic energy in the field. As $\dot{\phi} \approx 0$, potential energy dominates and accelerated expansion occurs.

4.2.1 Application to Cosmology

For a flat FRW metric, the energy momentum can be computed from (3.18), (4.7), (A.2, A.3) as:

$$\rho = \frac{1}{\sqrt{\mathcal{L}}}\Big(\frac{\dot{\phi}^2}{2\mathcal{L}} + V\Big) \tag{4.15}$$

$$p = \sqrt{\mathcal{L}}\Big(\frac{\dot{\phi}^2}{2\mathcal{L}} - V\Big) \tag{4.16}$$

where the *lapse function*

$$\mathcal{L} = 1 - B\dot{\phi}^2\,, \tag{4.17}$$

is related to the time-time component of the disformed metric (4.1). We will further define the *disformal factor* as:

$$\mathcal{D} = B\dot{\phi}^2\,. \tag{4.18}$$

Whenever $\mathcal{D} \ll 1$ the model will behave essentially as quintessence.

The equation of motion for the field can be obtained by direct variation of the action (4.6) w.r.t ϕ, by substituting (4.15, 4.16) in the continuity equation 2.13 or substituting the explicit partial derivatives (A.2-A.5) in the Klein-Gordon equation in terms of p (3.22). We can write the result in a form analogous to the harmonic oscillator as

$$M\ddot{\phi} + 3FH\dot{\phi} + P = 0 \tag{4.19}$$

where the analogs of mass, friction and potential terms can be written in terms of the disformal factor and the lapse as [2]:

$$M = 1 + \mathcal{L}BV + \frac{1}{2}\mathcal{D} \tag{4.20}$$

$$F = \mathcal{L}[1 + \mathcal{L}BV - \frac{1}{2}\mathcal{D}] \tag{4.21}$$

$$P = [\frac{3}{4}\dot{\phi}^2 + \frac{1}{2}\mathcal{L}V]B_{,\phi}\dot{\phi}^2 + \mathcal{L}^2 V_{,\phi} \tag{4.22}$$

In addition to the disformal factor and the lapse, we find the *disformal-potential factor*

$$BV = B_0 e^{(\beta-\alpha)\phi/M_p} \tag{4.23}$$

and the dimensionfull $B_{,\phi}\dot{\phi}^2$ which is just proportional to $\mathcal{D}$ for our choice of B.

4.2.2 Tracking Behaviour

Since disformal quintessence reduces to usual quintessence in the limit $B \to 0$, it is possible to have a tracking stage as described in section 3.1.1. For this to happen B has to fulfil $\mathcal{D} \ll 1$ and $BV \ll 1$ during most of the cosmic evolution. We can see that both conditions hold simultaneously in that case. If $\mathcal{D} \approx 0$, (4.15, 4.16) reduce to the usual quintessence values and

$$\dot{\phi}^2 \approx 2\frac{1 + w_\phi}{1 - w_\phi} V \,. \tag{4.24}$$

Therefore V and $\dot{\phi}^2$ are of the same order of magnitude if the equation of state is not close to ± 1, as it is in the tracking regime $w_\phi \sim w_m$.

With no loss of generality, we can consider the case $\alpha > 0$ for which the field evolves towards larger values. If $\beta > 0$, the disformal and disformal-potential factors may grow enough to break the usual quintessence behaviour and end the scaling regime.

[2] These definitions are related to the coefficients in (3.22) by a factor of $\mathcal{L}^{5/2}$. We used the three methods described above as a cross check.

Equation 4.23 implies that BV may only become significant if $\beta > \alpha$. The same condition holds for $\mathcal{D}$ as we can see if we plug the values of the field and its derivative (with $w_\phi \approx w_m$ and $\rho_\phi \approx \Omega_\phi \rho(a)$)

$$\phi = -\frac{M_p}{\alpha} \log[\tfrac{1}{2}(1-w)\Omega_q \rho M_p^{-4}\ ] \tag{4.25}$$

$$\dot{\phi} = \sqrt{(1+w)\Omega_q \rho}\ , \tag{4.26}$$

in the disformal factor:

$$B\dot{\phi}^2 = 2^{\frac{\beta}{\alpha}} \left[\Omega_q \rho M_p^{-4}\right]^{1-\frac{\beta}{\alpha}} \propto a^{3(1-\frac{\beta}{\alpha})}\,. \tag{4.27}$$

We have substituted $w = 0$ in the second equality assuming that the field leaves the attractor during the matter era. Hence, $\beta/\alpha > 1$ is a necessary condition to end the scaling regime. It turns out to be more useful to discuss the behaviour of the model in terms of β/α instead of β.

Obtaining the right Ω_q

In a logarithmic plot, $\mathcal{D}(a)$ is a linear function with slope $\propto \beta/\alpha$ during matter era (eq. 4.27). The offset of this constant term is proportional to B_0 and we can thus use this parameter to shift the freeze out time when the field begins to dominate. Hence Ω_q will be a monotonous function of B_0 for any set of cosmological parameters[3]. and we can use it as a parameter of the model. The algorithm used to invert $B_0(\Omega_q)$ is described in appendix B.2.

4.2.3 Accelerated Expansion

We have investigated the conditions under which the presence of a non negligible disformal factor might toss the field out of the attractor. We will now investigate the behaviour of the field at the disformal transition when $\mathcal{D}$ and BV become important.

Figure 4.1 shows the behaviour of the model for different values of β/α. The departure from the attractor consists of a slow down of the field (top plots), which is more significant and quicker for higher values of β/α. It can also be seen in the change in the equation of state and the dark energy fraction evolution (bottom plots). A glance at $w_\phi(a)$ reveals that high values are likely to be preferred by observations since they can efficiently imitate a cosmological constant. We will therefore concentrate on the case $\beta \gg \alpha$ in the following discussion.

[3]There is a transient reduction of the energy fraction at freeze out, but it is too short to play any relevant role.

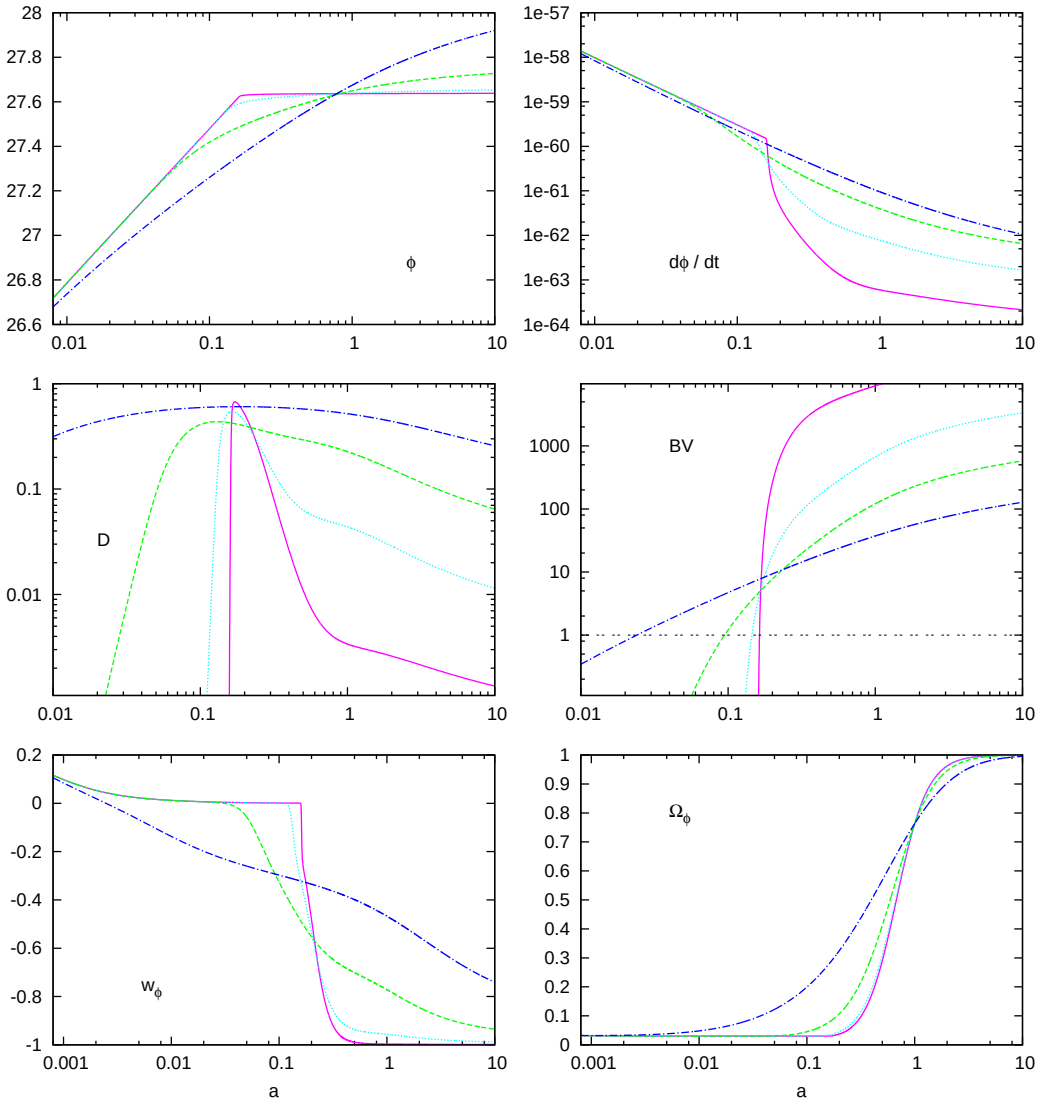

Figure 4.1: Behaviour of the model. ϕ and $\dot{\phi}$ in Planck units (first line), $\mathcal{D}$, BV (second line), w_q and Ω_q (third line) as a function of a for $\alpha = 10$. The values of β/α are 1.5 (dash-dotted dark blue), 3 (dashed green), 12 (dotted light blue) and 80 (purple). Note that the evolution has been extrapolated until $a = 10$.

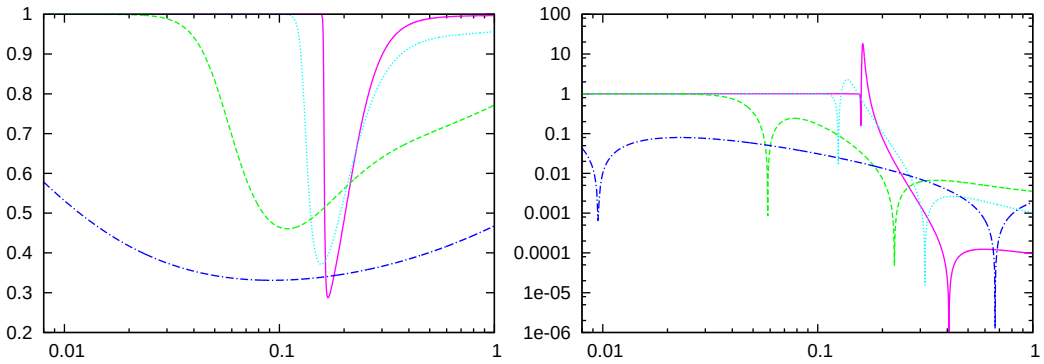

Figure 4.2: Terms in the Klein Gordon equation: $\frac{F}{M}/3$ (left) and $\left|\frac{P}{M}/V_{,\phi}\right|$ (right). They have been divided by the usual quintessence terms,3 and $V_{,\phi}$, to reflect the differences. The first plots shows the little correction in the friction term around freeze-out. The second shows the two disformal effects discussed in the text: The change of sign coming from the disformal potential (second line of eq. 4.31) and the BV^{-1} supression present in both terms. The parameters have the same values as in Figure 4.1.

The disformal factor depends on both $\phi, \dot{\phi}$ and has a nontrivial behaviour. It grows during the tracking period (eq. 4.27), reaches a maximum at the *freeze-out time* t_x[4], falls down rapidly until it reaches a certain value and then continues decreasing until present.

This behaviour can be understood in terms of the metric interpretation of the disformal factor, which implies that $\mathcal{D} < 1$ at any time. Otherwise the inverse disformal metric would run into a singularity and many quantities would blow up, notoriously the energy density (4.15). A slow down of the field is therefore to be expected whenever $\mathcal{D}$ approaches unity. No similar bound can be put on the potential-disformal factor. Since BV grows exponentially with ϕ, it can overcome the small velocity at slow roll and reach large values after the freeze out.

Equation for the Field

If $\beta \ll \alpha$, the disformal factor is well below one except during some interval around freeze out. This observation suggest an expansion to first order in $\mathcal{D}$ to gain some intuition about the model. Let us analyse the equation of motion (4.19) in the more

[4]It is possible to define the freeze-out time as the point for which $\mathcal{D}$ peaks or the equation of state changes, but these definitions fail if β/α is not large enough. An alternative possibility is to define t_x by $BV(t_x) = 1$, which is more general but fails to reflect the departure from the attractor in the low β/α case.

usual form:

$$\ddot{\phi} + 3\frac{F}{M}H\dot{\phi} + \frac{P}{M} = 0\,. \tag{4.28}$$

For the friction term we get a simple correction with respect to the usual quintessence case ($F/M = 1$)

$$\frac{F}{M} = 1 - \mathcal{D} + \mathcal{O}(\mathcal{D}^2)\,. \tag{4.29}$$

The order of magnitude of the friction term is given by the Hubble factor, and can be estimated as

$$H\dot{\phi} \sim \frac{\rho_q}{M_p}\left(1 + \frac{\rho_m}{\rho_q}\right)^{1/2} \sim \left\{ \begin{array}{ll} \alpha\frac{\rho_q}{M_p} & (t < t_x) \\ \frac{\rho_q}{M_p} & (t > t_x) \end{array} \right. \tag{4.30}$$

since $\rho_q/\rho_m \sim \Omega_q \propto \alpha^{-2}$ at tracking and $\rho_m/\rho_q \sim 0$ well after the freeze out.

The expansion for the P/M term requires more care. Taking into account that $\dot{\phi}^2 B_{,\phi} = \beta\mathcal{D}/M_p$ and $V_{,\phi} = -\lambda V/M_p$ then

$$\begin{aligned} \frac{P}{M} = &-\frac{\alpha}{M_p}\frac{V}{1+BV}\left[1 + 3\mathcal{D}\frac{1-2BV}{2(1+BV)}\right] \\ &+\frac{\beta}{M_p}\mathcal{D}\frac{1}{2}\frac{\frac{3}{2}\dot{\phi}^2 + V}{1+BV} + \mathcal{O}(\mathcal{D}^2)\quad . \end{aligned} \tag{4.31}$$

The first line reduces to the usual $V_{,\phi}$ at early times, but it will receive an additional supression by the BV factor in the denominator growing large at later times. The second term in brackets is subdominant due to the factor $\mathcal{D}$. The order of magnitude of the first line of (4.31) is roughly

$$V_\alpha \sim \frac{\alpha}{1+BV}\,\frac{\rho_q}{M_p}\,. \tag{4.32}$$

The second line represents the purely disformal contribution to the potential. Its order of magnitude can be estimated in a similar way as

$$V_\beta \sim \frac{\beta\ \mathcal{D}}{1+BV}\frac{\rho_q}{M_p}\,. \tag{4.33}$$

Equations 4.30, 4.32, 4.33 make clear that the disformal transition is driven by the interplay between both potential terms. The transition starts when $|V_\beta| > |V_\alpha|$ and lasts until $|V_\beta| < |V_\alpha|$. This change in the sign of the potential produces the deceleration of the field, which is very efficient if $\beta \ll \alpha$. In our approximation, this conditions corresponds to

$$\mathcal{D} \sim \alpha/\beta\,. \tag{4.34}$$

We can see in the plots that the disformal factor stabilises approximately around this value in Figure 4.1. During the transition, the value of BV increases significantly,

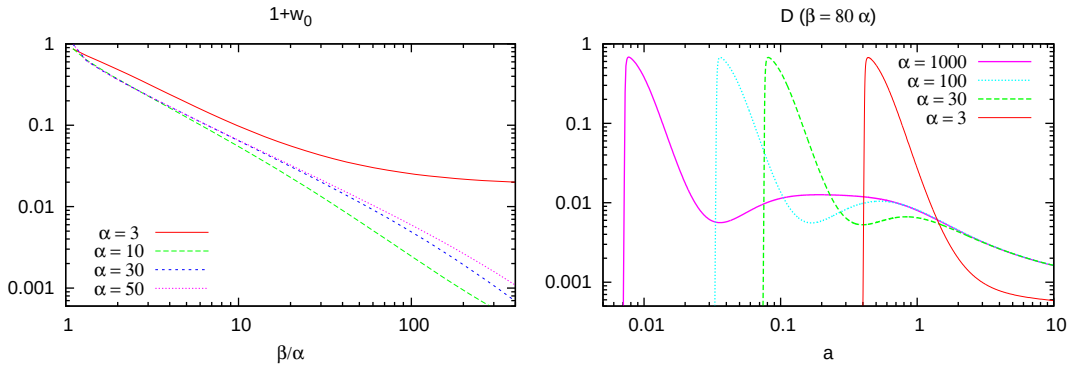

Figure 4.3: Disformal transition dependence on α. w_0 as a function of β/α for $\alpha = 3,\ 30$ (left). Evolution of the disformal factor for different values of α. Lower amounts of early dark energy require earlier freeze out times.

making the contribution of the potential negligible. We can identify the growth of this term with an increase in the "mass" of the field (4.20), in terms of the harmonic oscillator analogy given by the Klein-Gordon equation 4.19.

The later and softer slow down of the field would then be driven by the friction term, which does not suffer this supression. Figure 4.2 shows the behaviour of the friction and potential terms compared to the usual quintessence case and confirms the features discussed above.

Equation of State

Following the same procedure, we can compute the equation of state from equations 4.16, 4.15 to first order in $\dot{\phi}^2/V$ and $\mathcal{D}$ to be $w \approx -1 + \mathcal{D} + \frac{1}{2}\dot{\phi}^2/V$. At late times, when the kinetic energy is negligible, the equation of state becomes

$$w \approx -1 + \mathcal{D}\,, \tag{4.35}$$

and we expect that $w_0 + 1 \sim \alpha/\beta$ according to the discussion above. Figure 4.3 shows that this is the general trend for high values of α and β. For larger amounts of early dark energy the freeze out does not finish before the required Ω_ϕ is reached, as it becomes clear for the curve with $\alpha = 3$. Similar considerations apply for low values of β/α when the freeze out last long. This supports our considerations about the self adjustment of the disformal factor derived in the previous section and strongly links the properties of the accelerated expansion to the quotient β/α. Apparently the only role of α is to regulate the amount of early dark energy and therefore push the transition towards earlier times to compensate the larger period necessary to achieve Ω_ϕ today.

The previous considerations suggest that the model can not be distinguished from ΛCDM in the limit $\alpha \to \infty$ and $\beta/\alpha \to \infty$. The first condition ensures that the amount

of early dark energy is small enough to satisfy BBN, LSS and CMB constraints, while the second provides a very convenient equation of state at late times to fit the SNe data: $w(t > t_x) \approx -1$.

While the freeze out transition might be a clear observational signature of disformal quintessence, we expect this transient effect to be difficult to observe since it occurs at high redshifts ($z_x \gtrsim 5$) and is masked by the low fraction of dark energy if α is large enough. In chapter 6 we will study the growth of structure within this model and discuss possible observational implications.

4.2.4 On the Value of B

We have seen how disformal quintessence is able to achieve a late time ΛCDM-like behaviour in some limit. Besides, the existence of attractor solutions seems to solve one aspect of the coincidence problem, in the sense that, whenever the freeze out mechanism is triggered, the energy density of the field is only a factor α^{-2} apart from the matter density. On the other hand, the transition mechanism is determined by the model parameters with no connection to other circumstances in the present universe.

In the previous discussion, we have always tuned the value of B_0 to obtain the right amount of Ω_q at present. With our definitions of B and V an estimate can be obtained by using the condition $BV|_{a_x} \sim 1$

$$B_0 \sim \exp(-(\beta - \alpha)\phi_x/M_p) \sim \left(\frac{\rho_q(a_x)}{M_p^4}\right)^{\beta/\alpha - 1} \tag{4.36}$$

where we have used (4.25) in the second equality. Since $\rho_q(a) = \rho_m^{(0)}/(\alpha^2 a^3)$ at tracking, $\rho_0/M_p^4 \sim 10^{-120}$, and $a_x \sim 0.1$ for $\alpha \sim 10 \ll \beta$ we have roughly

$$B_0 \sim \left(10^{-120}\right)^{\beta/\alpha} \ . \tag{4.37}$$

Therefore we need a very small value of B_0, which becomes increasingly small for large values of β/α. [5]

Let us recall that we defined B_0 by requiring $V_0 = 1$ and we could in principle set it to unit by simply shifting the initial value of the field

$$B_0 \to B_0 e^{\beta\phi_0/M_p} \, , \tag{4.38}$$

$$V_0 \to V_0 e^{-\alpha\phi_0/M_p} \, . \tag{4.39}$$

[5]Note that B_0 is not an adimensional comparison between two scales: It is only meaningfull as a value in units of M_p^{-4} in (4.11). This choice is arbitrary and a more fundamental theory should be able to address the natural scale for B_0. But changing the units to a lower scale does not help at all, and actually the only way to get a order unity value for (4.37) would be to supposse a scale *higher* than M_p.

If we had chosen ϕ_0 to swallow (4.37), we would end up with a value of $V_0 \sim 10^{-120}$ (in Planck units) instead. It is also possible to encompass the parameter in a field offset difference between B and V, i.e. hold our usual definitions but assume

$$B_0 = e^{-\beta\phi_x} \, . \tag{4.40}$$

With this definition[6], ϕ_x is of a similar order of magnitude as the dynamical range of the field independently of β. We do not know the ultimate origin of the disformal transformation, however, it does not seem strange that the scalar field has two distinct regimes for $\phi \ll \phi_x$ and $\phi \sim \phi_x$.

[6]This is the approach we followed computationally to tune the fraction of dark energy, see appendix B.2.

Chapter 5

Observational Constraints

We now proceed to relate the model to astronomical observations. In order to do so, we performed a Monte Carlo Markov Chain analysis of the parameter space to obtain the posterior distribution. The study follows the lines of [43], where several simple models for dark energy are considered at the background level.

5.1 Astronomical Data

We used a combined analysis of Supernovae, Baryon Acoustic Oscillations and CMB shift parameter. In addition,we add a Gaussian prior on the value of the Hubble parameter obtained from the Hubble Space Telescope Key Project [44] $h = 0.72 \pm 0.08$.

It is important to keep in mind that the baryon acoustic scale and the CMB shift parameter are not directly measured quantities but rather obtained by implicitly assuming a ΛCDM cosmology. Therefore, they might lead to inconsistent results when applied to models with significant departures from Λ, as for example in modified gravity theories [45, 46].

If well we do not expect disformal quintessence to behave very differently from the concordance model as to question this results, we will take them as provisory. Our final objective will be to run a full MCMC simulation including first order perturbations and accounting for full CMB and LSS data.

5.1.1 The Union SNe Compilation

The union dataset [13] is the most recent available SNe compilation, made up by combining high quality high redshift data from the SCP, SNLS, ESSENCE and Hubble Space Telescope with older datasets. They also add a new sample of 8 nearby SNe, which causes a significant improvement in the statistics. The original sample, consisting of 414 SNe reduces to 307 after selection cuts, which are done in a systematic way

in order ensure the quality of the data (redshift, quality of the fit, number of datapoints, information about the colour and observation of a significant interval around peak luminosity are considered). Contrary to previous compilations, this procedure is standardised to avoid bias from human subjectivity.

Data analysis and search for systematics are done in a blind way. This is again to avoid the tendency to stop the analysis once the expected "right" answer is found. The amount of data contained in the sample allow a deep exploration of the systematics and many internal consistency checks that help validate the use of SNe 1a as standard candles[1]. Section 5 of [13] contains a deeper discussion of the systematic effects, which add to $\Delta M = 0.040$ mag for the whole sample and $\Delta M_i = 0.033$ mag for individual samples.

5.1.2 The Baryon Acoustic Peak

The value of the baryon acoustic scale we have included in our analysis was obtained by Eisenstein et al. in 2005 [15]. We have not included more recent results from Percival et al. (2007) [47] because there have been some doubts on their consistency. In particular, the two datapoints at $z = 0.2, 0.35$ seem to be incompatible with a ΛCDM cosmology when other measurements are taken into account.

In order to do so they explored the power spectrum of the luminous red galaxy sample from Sloan Digital Sky Survey. This sample is very convenient since it uses the same type of galaxy at all redshifts. The sample is projected from redshift space into comoving coordinates and binned afterwards. In order to do so, a flat ΛCDM cosmology is assumed. From this distribution, the two point correlation function is calculated. The baryon acoustic scale is well in the linear regime, but effects of nonlinear clustering tend to broaden the peak and increase the uncertainties. Modified growth, redshift distortions and scale dependent galaxy bias are taken into account by extrapolating the results from N-body simulations.

Current BAO determinations are not able to distinguish the radial and the angular scales. To model the mixing between both, the dilation scale is defined as the cube root of the radial dilation times the square of the comoving angular diameter distance $[D_a(z)^2 z H(z)^{-1}]^{1/3}$. Results are quoted in terms of the function $A(z) = D_V(z)\frac{\sqrt{\Omega_m} H_0^2}{z}$ at the fiducial redshift of the survey $z = 0.35$. For a flat spacetime it reads

$$A(z) = \sqrt{\Omega_m} E(z)^{-\frac{1}{3}} \left[\frac{1}{z} \int \frac{dz'}{E(z)} \right]^{\frac{2}{3}} , \tag{5.1}$$

and the observed value is $A(0.35) = 0.469 \pm 0.017$ with one sigma error.

[1] As an example, the parameters α, β from (2.17) can be studied in the high/low redshift regions or in different colour intervals. The result is that β is almost independent but α has a significant z dependence. However, its small coefficient $\langle 1 - s \rangle = 0.04$ makes this difference unimportant for the analysis.

The *AnalyzeThis!* class within CMBeasy [48, 49] provides a function to compute the Gaussian likelihood associated with this quantity, including corrections associated with the spectral index and possible modifications of the sound horizon due to early dark energy.

5.1.3 The CMB Shift Parameter

The CMB spectra contains information on the distance to the decoupling epoch, codified in the locations of peaks of the acoustic oscillations. The shift parameter of the CMB is described in section 5.4 of [50]. It is proportional to the angular diameter distance to the decoupling epoch divided by the Hubble horizon size at decoupling $d_A(z_*)H(z_*)$. Its value is given by

$$R = \sqrt{\Omega_m} \int_0^{z_*} \frac{dz}{E(z)} \,. \tag{5.2}$$

The WMAP 5-year result gives a value $R = 1.710 \pm 0.019$ with one sigma error.

In order to calculate the associated likelihood, we incorporated a function to calculate a Gaussian likelihood with $\chi^2 = 0.5(R - 1.710)^2/0.019^2$ to be added to the rest of the data. In addition to the shift parameter, the WMAP also gives the quotient of the angular diameter distance to decoupling to sound horizon at decoupling.

5.2 MCMC Analysis

We performed a Markov Chain Monte Carlo exploration of the parameter space with the driver included in CMBEasy. The algorithm as well as an outline of the procedure are briefly discussed in appendix C.

The relevant parameters for this background study are Ω_m, Ω_ϕ, h and the two parameters for the model, that we will introduce as α β/α. The baryon content does not significantly change the BAO results in the range allowed by WMAP data [15]. We set the remaining parameters to the WMAP best likelihood fit described in [51]. Ω_ϕ was set by demanding flatness, while we gave the range for h and Ω_m by extending the WMAP5 constraints. The lower bound on α was chosen to ensure the existence of the scaling solution. Dark energy domination requires $\beta/\alpha > 1$. This higher bounds were chosen by observing the dependence of the χ^2 with the parameters so that both limits are well in the region where there is no further sensitivity. Initial conditions for the field were given such that it lays in the radiation attractor in accordance to the scenario we want to study. The flat priors are summarised in table 5.1.

The code employed four chains using adaptive stepsize algorithm and stepsize freeze-out after convergence is reached. The Gellman Rubin convergence test described in appendix C was set up to use at least 30 points per chain. The whole run took about 20

Parameter	Min	Max	Δ_0
$\Omega_m h^2$	0.1	0.5	0.02
h	0.5	0.9	0.032
α	2	20	1.0
β/α	1.1	40	2.0

Table 5.1: Flat priors for the MCMC analysis.

hours in a LAM/MPI environment using five processors at the Institut für Theoretische Physik of the University of Heidelberg. A total of 28700 models were accepted and used for the analysis.

5.2.1 Results

Figure 5.1 displays the confidence regions obtained by the run. It can be seen that the bounds are not very stringent in the range of parameters we have chosen, and there is very little interdependence between α and β/α with the exception of the lowest corner. This happens because of the combined effect of high amount of early dark energy and slow freeze out (see Figure 4.3).

Figure 5.2 displays the one parameter likelihood. This plots makes very noticeable how weak do the constraints become for high values of α and β. The constraints obtained are summarised in table 5.2.

Parameter	Max. Likelihood	68% C.L.	95% C.L.
Ω_m	0.272	$^{+0.016}_{-0.015}$	$^{+0.031}_{-0.030}$
h	0.73	± 0.08	$^{+0.15}_{-0.14}$
α	10.0	$^{+7.9}_{-1.5}$	> 7.25
β/α	31.9	$^{+5.4}_{-15.0}$	> 9.5

Table 5.2: Results from the MCMC. The constraints are obtained from the polynomial fits to the binned distribution shown in Figure 5.2. The best fit model corresponds to $\Omega_m = 0.27$, $h = 0.71$, $\alpha = 10.8$, $\beta/\alpha = 38.65$.

The above constraints were actually calculated by considering the 68 and 95% area under the curves. This lead to a slight dependence on the parameter range chosen for the fit in the absence of an upper bound. For the intervals reduced to half of their initial sizes the two sigma bounds were pushed to $\alpha > 6.47$ and $\beta/\alpha > 7.5$.

Contrary to our expectations, preferred values of α are close to 10 and not higher. This finding is statistically uncertain and should not be interpreted as a preferred

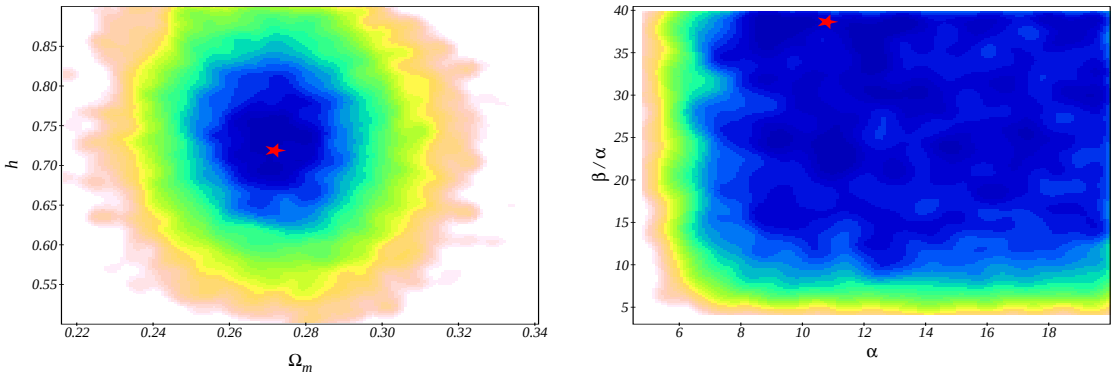

Figure 5.1: Contours corresponding to the 68 (blue), 95 (turquoise) and 99 (pink) percent confidence level regions in the $\Omega_m - h$ and $\alpha - \beta/\alpha$ planes. The red stars locate the best fit model.

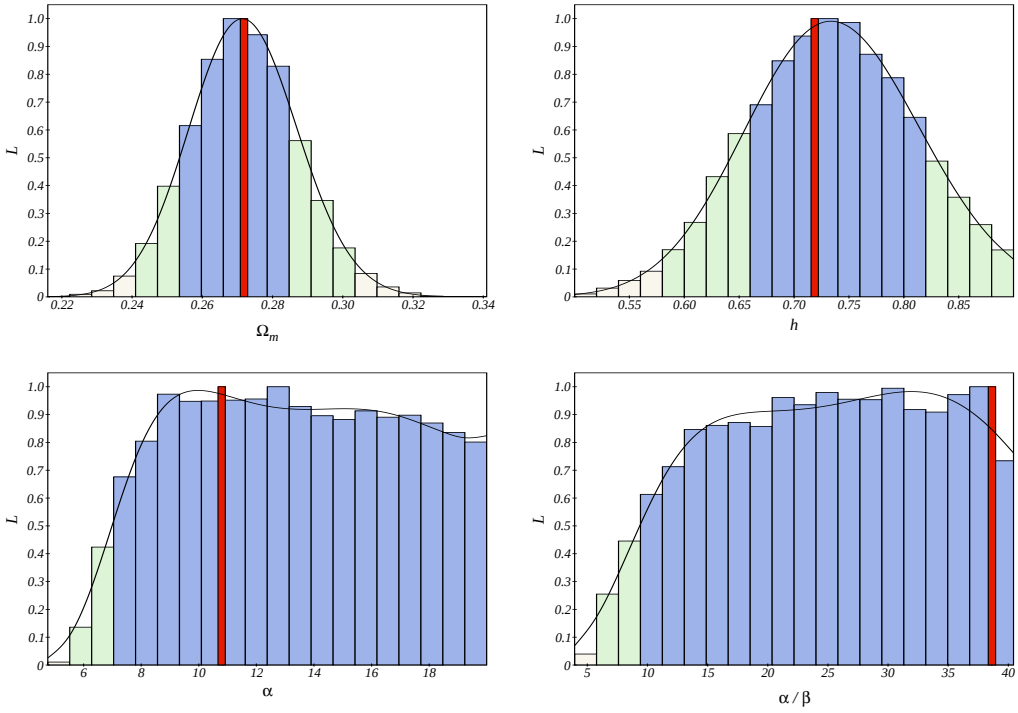

Figure 5.2: One parameter marginalised projection of the likelihood for Ω_m, h, α and β/α. The distribution has been binned and fitted to a polynomial. Red bars show the best fit model. All plots have been obtained with CMBeasy GUI.

amount of early dark energy, but rather as the lack of sensitivity of our probes above a certain threshold. Similarly, the apparent decrease of the likelihood for higher values of beta might be an border effect caused by the rejection of models with $\beta/\alpha < 40$ or a failure of the polynomial to fit the binned distribution, not the onset of a lower likelihood region. This was confirmed by direct exploration of the likelihood for higher values of β/α.

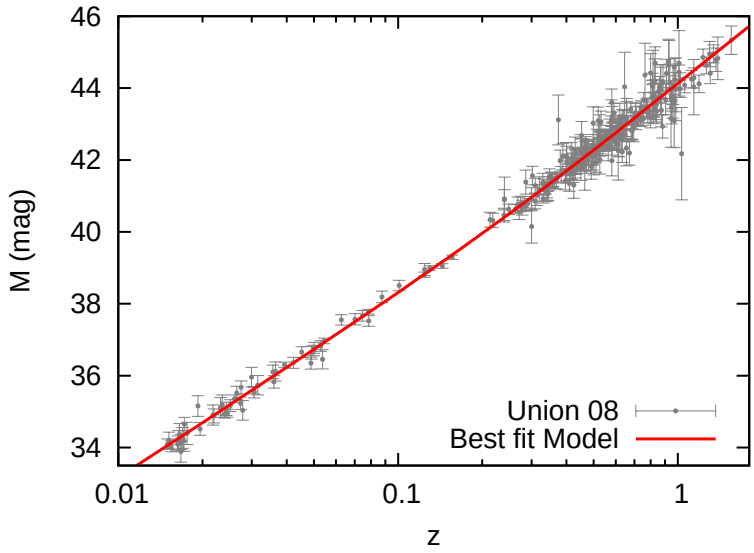

Figure 5.3: Apparent magnitude compared with the Union supernovae data for the best fit model $\Omega_m = 0.27$, $h = 0.71$, $\alpha = 10.8$, $\beta/\alpha = 38.65$.

Hopefully, new MCMC explorations including linear perturbations and different sets of observations will help to tighten the constraints yet found. Section 6.3 will describe how the CMB and matter power spectrum might be used for this purpouse and in section 7.1.1 will ennumerate other posible data sets to help in this task.

Chapter 6

Linear Perturbations

This chapter will consider the theory linear perturbations in the synchronous gauge. We will first derive the relevant equations, analyse their behaviour and discuss possible effects in the CMB anisotropies and the matter power spectrum. The description of the modifications in CMBEasy that were necessary for this study are sketched in appendix B.3 together with the tests that were performed. For the sake of concision we will only discuss those issues in cosmological perturbation theory that are specific to minimally coupled scalar fields. A thorough description of cosmological perturbations in this gauge can be found in [52].

6.1 Equations in the Synchronous Gauge

The synchronous gauge is specified by the line element with no perturbation in the time components $\delta g_{0\mu} = 0$

$$ds^2 = a^2(\tau)\left[-d\tau^2 + (\delta_{ij} + h_{ij})\, dx^i dx^j\right] . \tag{6.1}$$

In this gauge free falling observers will remain in the same comoving position, as will be the case for dark matter particles. Equation 6.1 does not completely fix the coordinates. As a consequence some solutions to the equations may correspond to the excitation of unphysical (gauge) degrees of freedom. These modes can be avoided by appropriately choosing the initial conditions[1]. The gauge choice also affects the behaviour of perturbations on super horizon scales, but these produce no observable effects.

The spatial perturbation for scalar modes is determined by the following Fourier

[1]Since disformal quintessence is indistinguishable from minimal quintessence at early times there is no need to modify the initial conditions for the field.

expansion in terms of the comoving wavevectors $\vec{k}$

$$h_{ij}(\mathbf{x},\tau) = \int d^3k e^{i\mathbf{k}\cdot\mathbf{x}} \left[\hat{k}_i\hat{k}_j h(\mathbf{k},\tau) + 6\left(\hat{k}_i\hat{k}_j - \frac{1}{3}\delta_{ij}\right)\eta(\mathbf{k},\tau)\right], \tag{6.2}$$

where $\mathbf{k} = k\hat{k}$. In the linear theory each mode evolves independently and we will therefore drop the explicit dependence on k. Furthermore, scalar modes are also independent from vector and tensor modes to this order and these will not be considered.

6.1.1 Einstein equations

The action for the whole theory is given by

$$S = \int d^4x\mathcal{L} = \int d^4x\sqrt{-g}\left\{\frac{R}{16\pi G} + p(X,\phi) + \mathcal{L}_m\right\}, \tag{6.3}$$

where p is given by (4.7) with $A = 1$. Variation with respect to the inverse metric yields the first order Einstein equations

$$\delta G^{\mu}{}_{\nu} = 8\pi G\delta T^{\mu}{}_{\nu}\,. \tag{6.4}$$

The energy momentum part corresponds to

$$\delta T^0{}_0 = -\delta\rho\,, \tag{6.5}$$
$$\delta T^0{}_i = -T^i{}_0 = (\rho+p)v_i\,, \tag{6.6}$$
$$\delta T^i{}_j = \delta p\delta^i_j + \Sigma^i{}_j\,, \tag{6.7}$$

with $\delta\rho$ and δp the density and pressure perturbations, v the velocity and $\Sigma^i{}_j$ the anisotropic stress. These quantities need to be evaluated in the synchronous gauge for consistency.

Minimally coupled quintessence does not affect the gravitational part of the action, and therefore the left hand side of (6.4) will have the usual form. The time-time, time-space, space-space trace and space-space traceless equations in $k-$space are (see [52]):

$$\frac{1}{2}\mathcal{H}h' - k^2\eta = 4\pi Ga^2\delta\rho\,, \tag{6.8}$$
$$k^2\eta' = 4\pi Ga^2(\rho+p)\theta\,, \tag{6.9}$$
$$h'' + 2\mathcal{H}h' - 2k^2\eta = -24\pi Ga^2\delta p\,, \tag{6.10}$$
$$h'' + 6\eta'' + 2\mathcal{H}(h' + 6\eta') - 2k^2\eta = -24\pi Ga^2(\rho+p)\sigma\,, \tag{6.11}$$

where θ and σ are defined as

$$(\rho+p)\theta \equiv ik^i\delta T^0{}_i\;; \quad (\rho+p)\sigma \equiv -(\hat{k}_i\hat{k}_j - \delta^i_j)\Sigma^i{}_j\,. \tag{6.12}$$

The metric perturbations η, h are difficult to interpret. It is more useful to consider the gauge invariant gravitational potentials instead

$$\Psi = \frac{1}{2k^2}\left[\ddot{h} + 6\ddot{\eta} + \mathcal{H}(\dot{h} + 6\dot{\eta})\right] , \tag{6.13}$$

$$\Phi = \eta - \frac{1}{2k^2}\mathcal{H}(\dot{h} + 6\dot{\eta}) . \tag{6.14}$$

Energy-Momentum Tensor

As we saw in section 3.2, the energy momentum tensor for general quintessence is given by:

$$T_{\mu\nu} = p\ g_{\mu\nu} - p_{,X}\phi_{,\mu}\phi_{,\nu} . \tag{6.15}$$

The first order components are obtained by expanding to first order in $\delta\phi$ and $\dot{\delta\phi}$. Metric perturbations would enter into these expressions only via the lapse perturbation which is set to zero in our gauge choice (6.1). The zero-zero component gives the value of the energy density perturbation

$$\delta\rho_\phi \;\; = \;\; -(p_{,X} - p_{,XX}\dot{\phi}^2)\dot{\phi}\dot{\delta\phi} - (p_{,\phi} + p_{,X\phi}\dot{\phi}^2)\delta\phi . \tag{6.16}$$

The coefficient of the first term will also appear in the Klein Gordon equation:

$$\mathcal{M} = -(p_{,X} - p_{,XX}\dot{\phi}^2) . \tag{6.17}$$

With this definition and using conformal time, the density perturbation reads

$$\delta\rho_\phi = \mathcal{M}\phi'\delta\phi'/a^2 + (p_{,\phi} + p_{,X\phi}(\phi'/a)^2)\delta\phi . \tag{6.18}$$

The pressure and the velocity perturbation are respectively

$$\delta p_\phi = p_\phi\delta\phi - p_X\phi'\delta\phi'/a^2 , \tag{6.19}$$

$$(\rho + p)\theta_\phi = -p_{,X}\frac{k^2}{a^2}\phi'\delta\phi . \tag{6.20}$$

Computation of the off-diagonal part of the metric leads to the absence of anisotropic stress to first order in perturbation theory:

$$\Sigma^i_{\ j} = \mathcal{O}(\delta\phi^2) . \tag{6.21}$$

6.1.2 Klein-Gordon equation

The equation for the field is more simply obtained using cosmic time. The starting point is the Euler-Lagrange equation 3.21:

$$\nabla_\mu(p_{,X}\partial^\mu\phi) - p_{,\phi} = 0\,. \tag{6.22}$$

This expression contains the perturbed values of the field. We therefore need to expand it to explicitly separate the background coefficients, which will only depend on time, and the perturbations. The first term can be decomposed in two parts:

$$\begin{aligned} p_{,X}\nabla_\mu\partial^\mu\phi &= p_{,X}(\Box\phi - g^{\mu\nu}\Gamma^\alpha_{\mu\nu}\partial_\alpha\phi) \\ &= -p_{,X}(\ddot{\delta\phi} + k^2\delta\phi + 3H\dot{\delta\phi} + \frac{1}{2}\dot{h}\dot{\phi}) \\ &\quad -(\ddot{\phi} + 3H\dot{\phi})[p_{,X\phi}\delta\phi - p_{,XX}\dot{\phi}\dot{\delta\phi}]\,, \end{aligned} \tag{6.23}$$

$$\begin{aligned} (\partial_\mu p_{,X})\partial^\mu\phi &= g^{00}(\dot{\phi} + \dot{\delta\phi})\partial_0(p_{,X} + p_{,X\phi}\delta\phi - p_{,XX}\dot{\phi}\dot{\delta\phi}) \\ &= [\dot{p}_{,XX}\dot{\phi}^2 + p_{,XX}\dot{\phi}\ddot{\phi} - p_{,X\phi}\dot{\phi} - \dot{p}_{,X}]\dot{\delta\phi} \\ &\quad + p_{,XX}\dot{\phi}^2\ddot{\delta\phi} \;-\; \dot{p}_{,X\phi}\dot{\phi}\delta\phi\,. \end{aligned} \tag{6.24}$$

In the above expressions all quantities are background-valuated whenever an explicit perturbation term multiplies it. The last term reads

$$-p_{,\phi} = p_{,X\phi}\dot{\phi}\dot{\delta\phi} - p_{,\phi\phi}\delta\phi \tag{6.25}$$

Adding the previous expressions and grouping terms with factors of $\delta\phi$, $\dot{h}$, $\dot{\delta\phi}$ and $\ddot{\delta\phi}$ leads to

$$\begin{aligned} \left(p_{,X} - p_{,XX}\dot{\phi}^2\right)\ddot{\delta\phi} + \left[3H(p_{,X} - p_{,XX}\dot{\phi}^2) + \dot{p}_{,X} - \dot{p}_{,XX}\dot{\phi}^2 - 2\dot{p}_{,XX}\dot{\phi}\ddot{\phi}\right]\dot{\delta\phi} \\ +\tfrac{1}{2}p_{,X}\dot{h}\dot{\phi} + \left[p_{,X}\tfrac{k^2}{a^2} - p_{,X\phi}\Box\phi + \dot{p}_{,X\phi}\dot{\phi} + p_{,\phi\phi}\right]\delta\phi\,, = 0 \end{aligned} \tag{6.26}$$

where $\Box\phi = -\ddot{\phi} - 3H\dot{\phi} = -(\phi'' + 2\mathcal{H}\phi')/a^2$. There are several occurrences of $\mathcal{M}$ and its time derivative in the first line. The equation renders simpler if those are explicitly written

$$\begin{aligned} \mathcal{M}\ddot{\delta\phi} + \left[3H\mathcal{M} + \dot{\mathcal{M}}\right]\dot{\delta\phi} + \tfrac{1}{2}p_{,X}\dot{h}\dot{\phi} \\ + \left[p_{,X}\tfrac{k^2}{a^2} - p_{,X\phi}\Box\phi + \dot{p}_{,X\phi}\dot{\phi} + p_{,\phi\phi}\right]\delta\phi = 0 \end{aligned} \tag{6.27}$$

The conformal time version follows by changing the time variable in the derivatives

$$\begin{aligned} \mathcal{M}\delta\phi'' + \left[2\mathcal{H}\mathcal{M} + \mathcal{M}'\right]\delta\phi' + \tfrac{1}{2}p_{,X}h'\phi' \\ + \left[p_{,X}k^2 + (\phi'' + 2\mathcal{H}\phi')p_{,X\phi} + p'_{,X\phi}\phi' + a^2p_{,\phi\phi}\right]\delta\phi = 0\,. \end{aligned} \tag{6.28}$$

We checked that our results in equations 6.18, 6.19, 6.20, 6.28 were in agreement with the ones exposed in section E of [53] for the more general Lagrangian density $f(R, X, \phi)$.

6.2 Evolution

Unlike in the background case, the equations for the perturbations are linear and each k mode will behave as a set of coupled harmonic oscillators with time varying coefficients. The time variation given by the background expansion and the independence of the different wavelengths are assumed as long as perturbation theory holds. This correspondence between $\delta\phi$, η, h,... and point like particles can help to understand the behaviour of the perturbations. We will make use of this analogy in this section to understand the behaviour the scalar field.

The Klein-Gordon equation 6.28 for each k-mode can be written as

$$\delta\phi'' + \left[2\mathcal{H} + \frac{\mathcal{M}'}{\mathcal{M}}\right]\delta\phi' + \left[c_s^2 k^2 + m_\phi^2\right]\delta\phi + c_s^2\frac{1}{2}h_k'\phi' = 0\,. \tag{6.29}$$

where

$$\mathcal{M} = -[p_{,X} - p_{,XX}(\phi'/a)^2]\,, \tag{6.30}$$

$$c_s^2 = \frac{p_{,X}}{\mathcal{M}}\,, \tag{6.31}$$

$$m_\phi^2 = \frac{1}{\mathcal{M}}\left[(\phi'' + 2\mathcal{H}\phi')p_{,X\phi} + p'_{,X\phi}\phi' + a^2 p_{,\phi\phi}\right] \equiv \frac{\mathcal{V}^{(2)}}{\mathcal{M}}\,. \tag{6.32}$$

Each field perturbation will also contribute to the energy density, pressure and velocity perturbations that source the Einstein equations. These will ultimately backreact in the Klein-Gordon equation through the source term $c_s^2 h_k'\delta\phi'$, which represents the coupling to gravity. The velocity perturbation receives just a factor of $p_{,X} = c_s^2\mathcal{M}$ with respect to the usual quintessence case, while the pressure perturbation is just the first order expansion of the Lagrangian density. The energy density (6.18) contribution can be rewritten as

$$\delta\rho_\phi = \mathcal{M}\phi'\delta\phi'/a^2 + \mathcal{V}^{(1)}\delta\phi\,. \tag{6.33}$$

The kinetic contribution is modulated by $\mathcal{M}$. The potential energy contribution reads

$$\mathcal{V}^{(1)} = -(p_{,\phi} + p_{,X\phi}\dot{\phi}^2)\delta\phi\,. \tag{6.34}$$

6.2.1 Disformal Transition

Figure 6.1 shows the effects of the disformal transition in the terms above for different values of β/α. Not surprisingly, their behaviour turns out to be similar to the background case as some coefficients are also present in the background equation analysed in section 4.2.3 (Figure 4.1).

The coefficient of the kinetic energy perturbation $\mathcal{M}$ appears as well with the second derivative of the field equation 6.28. Therefore, it can be identified with the

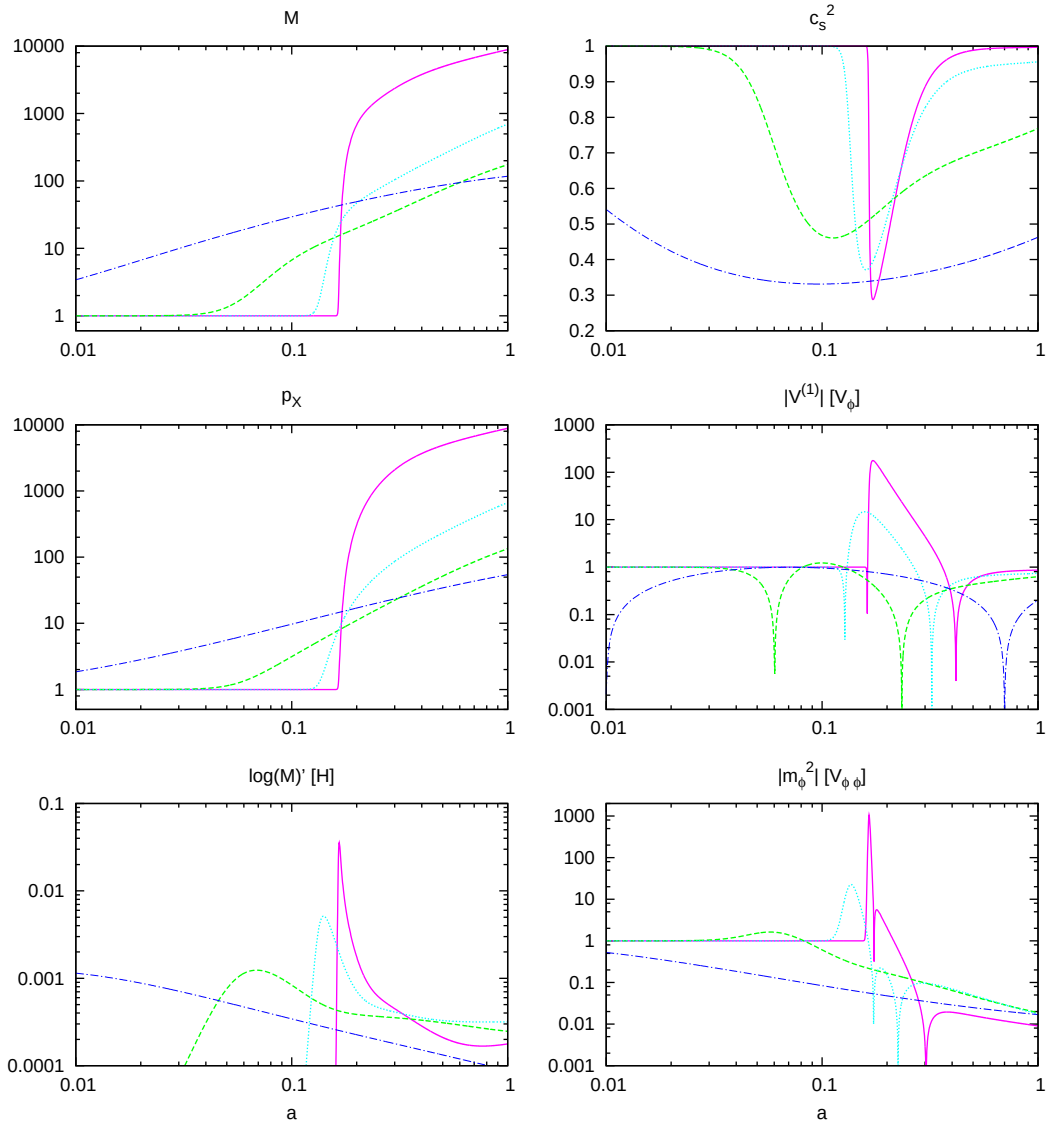

Figure 6.1: Terms in the Klein Gordon Equation (6.29) as a function of the scale factor for $\alpha = 10$ and β/α equal to 1.5 (dash-dotted dark blue), 3 (dashed green), 12 (dotted cyan) and 80 (violet). **First Line:** Mass of the field $\mathcal{M}$ and adiabatic speed of sound c_s^2. **Second Line:** Velocity perturbation term $p_{,X} = c_s^2\mathcal{M}$ and potential contribution to the energy perturbation $\mathcal{V}^{(1)}$. **Third Line:** Disformal quintessence terms in (6.29). $\frac{\mathcal{M}'}{\mathcal{M}}$ is displayed with respect to the usual friction term $\mathcal{H}$ and $m_\phi^2 = \frac{\mathcal{V}^{(2)}}{\mathcal{M}}$ to the usual quintessence potential term $V_{,\phi\phi}$.

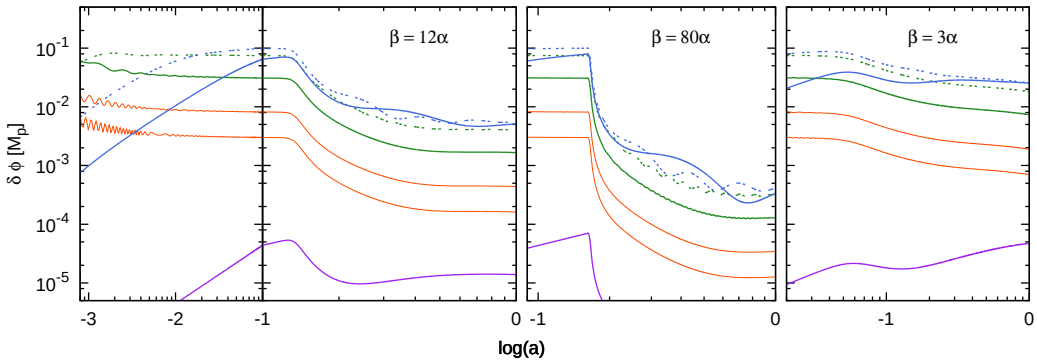

Figure 6.2: Evolution of the field perturbations for $\alpha = 10$ and $\beta/\alpha = 12, 80, 3$. The modes shown correspond to $k\tau_0 = 2000, 1000$ (orange), $k\tau_0 = 300$ (green), 100 (dashed green), $k\tau_0 = 30$ (dashed blue) and 10 (blue) and $k\tau_0 = 0.5$ (purple). Note that the longest wavelength mode (purple) corresponds to a super horizon scale today.

(time dependent) inertia of the k-modes[2]. $\mathcal{M}$ is proportional to the M coefficient which played the same role in the background equation for the field (4.19). Its value is very close to one at tracking and increases when the freeze out of the field occurs. This increase of the "inertia" for both the homogeneous field and the perturbations is in agreement with expectations. It makes increasingly difficult to produce changes in the field after the disformal transition.

The term $\mathcal{V}^{(1)}$ in (6.33) generalises the potential energy perturbation $V_{,\phi}$. It also represents the force acting on ϕ in the background Klein-Gordon equation (4.19)[3] responsible for the disformal transition and therefore experiences a change of sign. The second change of sign happens when the usual potential term takes over the disformal one.

A logarithmic derivative of $\mathcal{M}$ appears in the friction term of equation 6.29. This contribution is naturally understood on grounds of kinetic energy conservation. We can see in Figure 6.1 that this variation is negligible compared to the usual Hubble damping term. Contrarily to what happened in the background case, the $\mathcal{H}$ term is not modified and the expansion will generically act as a friction on the dark energy perturbations.

The usual potential term $V_{,\phi\phi}$ in the Klein-Gordon equation is generalised to $\mathcal{V}^{(2)}$. The analogy of the field mass is given by its ratio to the inertia $\mathcal{M}$. m_ϕ^2 is a measure of the restoring force acting on the field and hence of its oscillatory properties. For the case of high β/α the restoring force grows quickly first driving $|\delta\phi|$ towards a lower

[2]This "mass" of the mode should not be confused with the physical mass of the field m_ϕ which determines its minimum excitation energy and propagation properties.

[3]It is proportional to the potential term P which was described in section 4.2.3.

value. The subsequent evolution flips the sign of the potential, thending to push it away from its equilibrium position. However, the increase of $\mathcal{M}$ has by this time reduced the force considerably. After some time, the attractive nature is restored.

This variations on the potential term are reflected in the behaviour of the field perturbations, as can be seen in Figure 6.2. For the first curve ($\beta = 12\alpha$) the field value experiments a decrease, which is seen to be steeper in the next case due to the higher value of β/α. Both represent the reaction to the sudden increase in the field mass. The third case corresponds to a smooth transition due to a low value of β/α for which the reaction is much less pronounced.

The speed of sound has been defined in analogy with the wave equation ($\ddot{\chi}+c_s^2k^2\chi = 0$) as the quotient between the second time derivative and the k^2 term. It also multiplies the interaction term with gravity ($c_s^2\dot{h}_k\dot{\phi}$) and therefore modulates all the k dependence in the field equation. As in the wave equation, it measures of how fast the perturbations are able to propagate within the fluid and is hence an indicator of the efficiency of dark energy clustering. Usual quintessence and cold dark matter have speed of sound equal to one and zero respectively. The value for disformal quintessence is equal to the quotient F/M appearing on the background field equation (4.19), i.e.

$$c_\phi^2 = \mathcal{L}\frac{1 + BV\mathcal{L} - \mathcal{D}/2}{1 + BV\mathcal{L} + \mathcal{D}/2}\,. \tag{6.35}$$

It can be seen that $0 < c_s^2 < 1$ by recalling that $BV > 0$, $0 < \mathcal{D}, \mathcal{L} < 1$. Hence neither superluminal motion nor instabilities can arise. Figure 6.1 shows how the disformal transition produces a departure from $c_s^2 = 1$. The speed of sound reaches lower values for high β/α. However, low β/α make the deviation last longer and recover at a lower than value of c_s^2. This variation with respect to usual quintessence can produce an increase in the efficiency of dark energy clustering.

6.2.2 Dark Energy Clustering

The field variable determines the behaviour of the dark energy, but the effects of the perturbations will be ultimatelly given by the density perturbation (6.33) in term of $\delta\phi$ and $\delta\phi'$[4]. It is conventional to define the dark energy power spectrum as

$$P_k(\tau) = \frac{\delta^2(\tau)}{k^3}\,, \tag{6.36}$$

where δ is the the density perturbation, in our case $\delta\rho_\phi/\rho_\phi$. Linearity of the equations implies that the power spectrum can be arbitrarily normalised. Figure 6.3 shows the power spectrum at $z = 0$ as a function of $k\tau_0$ where is the conformal time at present is $\tau_0 \approx 14300$ Mpc. The tendency is towards a more efficient clustering for the models

[4]We will not discuss the velocity and pressure perturbations for the sake of brevity.

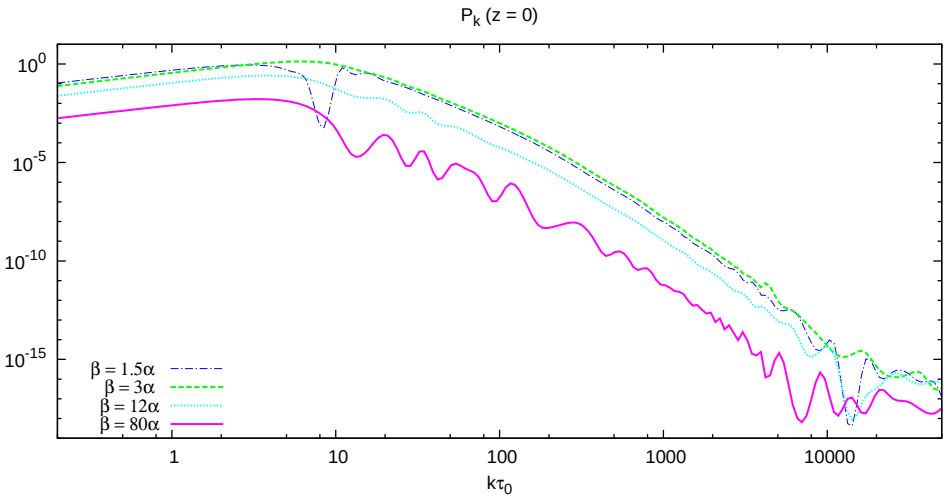

Figure 6.3: Dark energy power spectrum today for $\alpha = 10$ and different values of β. It can be seen how the lower values of β lead to more efficient dark energy clustering. In any case, the dark energy perturbations remain several orders of magnitude below the dark matter perturbations. The decrease in the spectrum for $\beta/\alpha = 1.5$ around $k\tau \sim 10$ probably corresponds to a change of sign of this particular mode close to present time.

with low values of β/α. This effect is likely due to the lower value of the speed of sound and the different equation of state.

Figure 6.4 shows the time evolution of some modes. Perturbations entering the horizon before the freeze out of the field tend to keep a rather constant average value. The transition produces oscillations intermediate wavelengths and a change of sign of the long scales including super-horizon. This does not represent a violation of causality, but a reaction to the background[5]. The cluster dependence on β/α mentioned above becomes particularly clear by comparing the top and bottom plots. It is also seen that the energy density perturbation varies rather slowly apart from the change of sign experienced after the transition and at later times. Hence the fast variation of the field observed in Figure 6.2 compensates for change of $\mathcal{V}^{(1)}$ and $\mathcal{M}$ keeping the value of the density perturbation within the same range.

6.3 Relation to Observations

Dark energy density perturbations will in turn affect the gravitational potentials which determine the growth of matter and the integrated Sachs-Wolfe effect seen on low

[5]It is actually similar to the change experienced by the large scale gravitational potentials at the radiation-matter domination crossing.

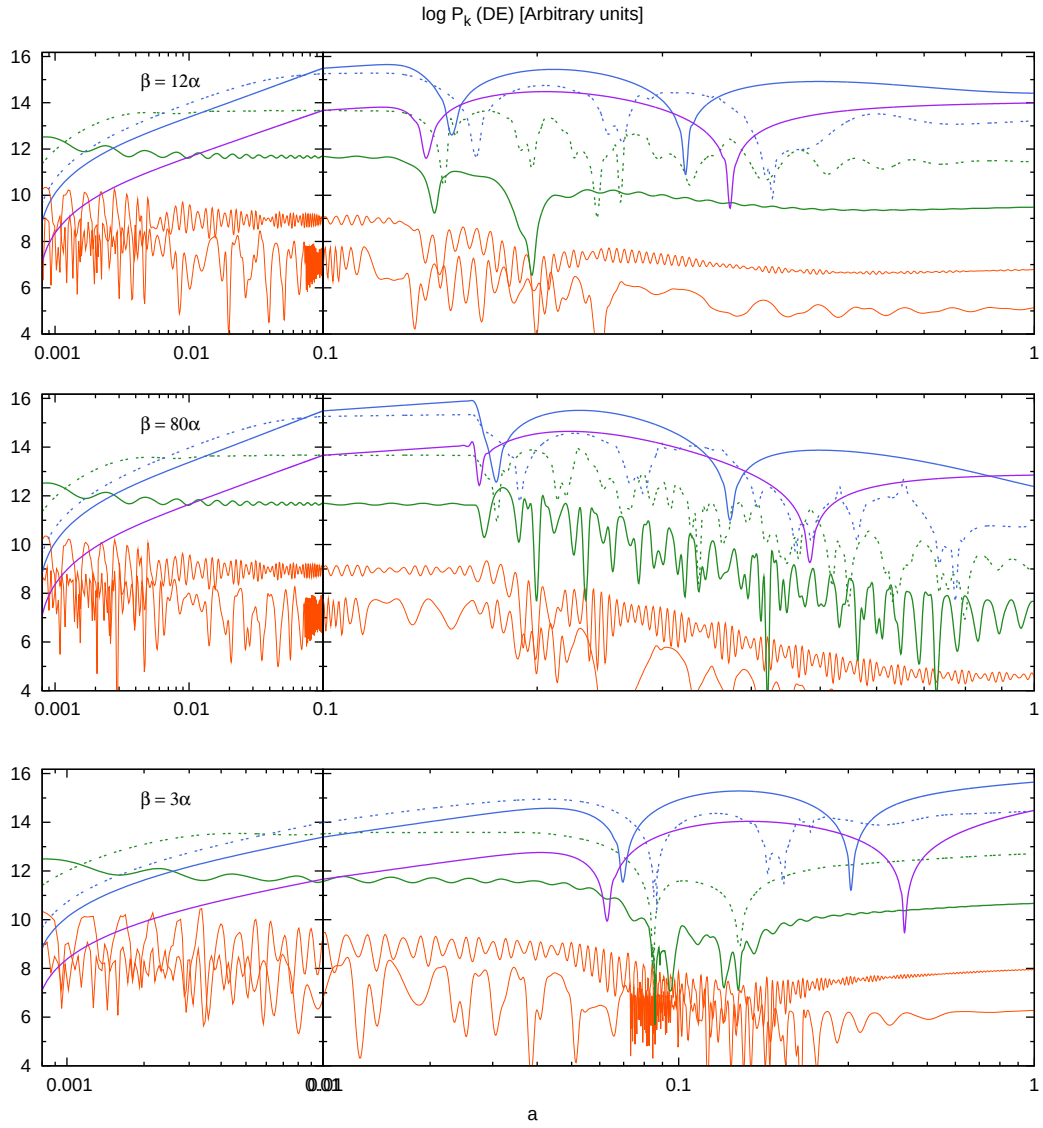

Figure 6.4: Dark energy power spectrum as a function of time for $\alpha = 10$ and different values of β. The lines correspond to $k\tau_0 = 2000, 1000$ (orange), $k\tau_0 = 300$ (green), 100 (dashed green), $k\tau_0 = 30$ (dashed blue) and 10 (blue) and $k\tau_0 = 0.5$ (purple). Normalisation is arbitrary but common.

multipoles of the CMB. In the ΛCDM model structure growth occurs mainly during the period in which matter dominates the density of the universe. The gravitational potentials Φ, Ψ are flat in this period and inhomogeneities grow as $\delta \propto a$ for the CDM and baryon species [2]. The late time accelerated expansion tends to wash out the potentials and avoid further growth of structure, erasing the inhomogeneities on large

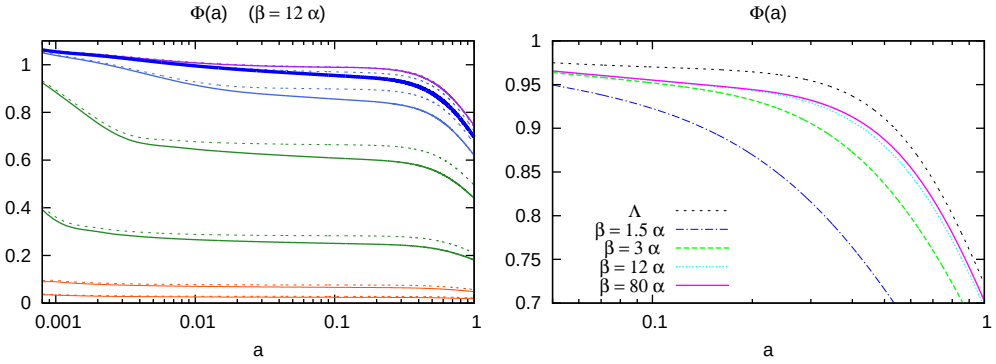

Figure 6.5: Gravitational potential Φ. The modes shown correspond to $k\tau_0 = 2000, 1000$ (orange), $k\tau_0 = 300, 100$ (green), $k\tau_0 = 30, 10$ (blue) and $k\tau_0 = 0.5$ (purple). **Left:** Behaviour of the gravitational potential for $\alpha = 10, \beta = 12\alpha$ and the scales shown in figure 6.4. The dashed lines are the equivalent modes for ΛCDM . **Right:** The large scale mode $k\tau_0 = 10$ (thicker line on the left) has been plotted at late times for different values of β. Potentials have been normalised to the value of Ψ on long scales at early times.

scales[6]. This behaviour can be seen in the dotted lines corresponding to ΛCDM in Figure 6.5.

Disformal quintessence introduces at least three features that cause departure from the standard cosmological model:

1. Certain amount of early dark energy proportional to α^{-2}. This departure of matter domination makes clustering less efficient at early times due to the tendency of the field to remain homogeneous on small scales.

2. Higher equation of state after the transition, with $1 + w \approx +\mathcal{D} \sim \alpha/\beta$. A lower expansion rate erases the potentials less efficiently, but acts for a longer time.

3. Speed of sound lower than one after the transition. Lower values of c_s^2 are likely to produce more efficient clustering and mimic the behaviour of matter to a certain extent.

The first effect causes the slight slope of the potentials seen before the freeze out of the field (left plot of Figure 6.5). It can be avoided by a sufficiently low amount of the early dark energy fraction i.e. if α is high. The second and third effects are seen after the transition and are difficult to disentangle. In any case both represent a

[6]This applies for linear perturbation theory. Nonlinear structures are bound gravitationally and are stable against the accelerated expansion.

more radical departure from Λ whenever β/α is low as becomes from the second plot in Figure 6.5 [7].

6.3.1 Cosmic Microwave Background

The three effects previously discussed are likely to affect the shape of the CMB spectrum. Departures from ΛCDM do change the spectra through modification of the angular diameter distance and the integrated Sachs-Wolfe effect produced by the evolution of the gravitational potentials at late times.

There are however two subtleties which difficult the observational distinction of the different models by using the CMB. The first is the large uncertainty present in the low multipole region of the spectrum (cosmic variance)[8]. It is then difficult to obtain significant constraints from the low l region unless there are significant deviations. The second is the large set of parameters that affect the shape of the spectrum [54]. If the angular shift produced by the late accelerated expansion is not very large, it can be corrected by a slight readjustment of h, n_s Ω_b and Ω_m. Since the spectrum obtained is proportional to the initial perturbations, there is also freedom to reescale it by a multiplicative constant corresponding to a change in the amplitude of the initial perturbations A_s. This amount of freedom and the delicate interplay among the parameters make it difficult to establish a priori how CMB data will be able to constraint the model. A MCMC analysis becomes necessary to address this question properly.

The importance of the initial amplitude of the perturbations can be seen by comparing the two plots in Figure 6.6. The only curve that can be clearly ruled out after reescaling is the one corresponding to $\alpha = 3$, which represents a huge early dark energy fraction (38%). For the remaining curves the rescaling is lower than 5%. Figure 6.7 shows the dependence with β/α. The only noticeable aspects are the shift of the parameters and the higher ISW effect for low values of β/α. This features are likely to be related to the behaviour of the background expansion rather than to the clustering properties of the field. The angular diameter distances are modified by the lower equation of state and the ISW plateau is raised by the longer decay of the gravitational potentials (see Figure 6.5). We checked that this behaviour was similar also when significant amounts of dark energy were present, even for $\alpha = 3$.

[7] $c_s^2 < 1$ would actually help to mask the amount of early dark energy if that were the case *before* dark energy domination. In reference [14] the study of large scale anisotropies considering constant values of the equation of state and speed of sound is undertaken. The conclusion is that there is little dependence on the value of c_s^2.

[8] The low amount of values of m $(2l+1)$ for lower multipoles produces a large statistical uncertainty in the measured $C_l = \langle |a_{lm}|^2 \rangle$.

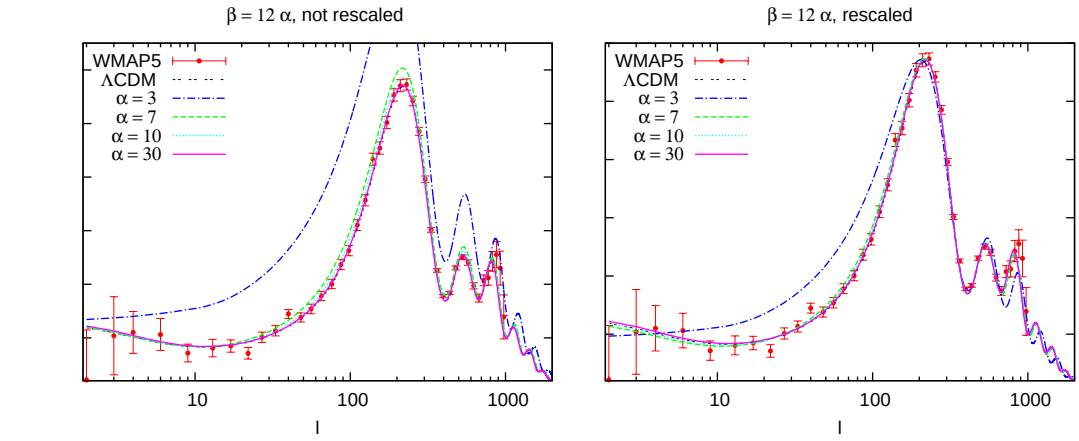

Figure 6.6: CMB spectra dependence on α. **Right:** Spectra using the same normalisation. **Left:** Rescaled spectra for $\beta/\alpha = 12$ and different values of α. The rescaling factors were $0.72, 0.95, 0.98, 1$ for $\alpha = 3, 7, 10, 30$ with respect to ΛCDM initial amplitudes.

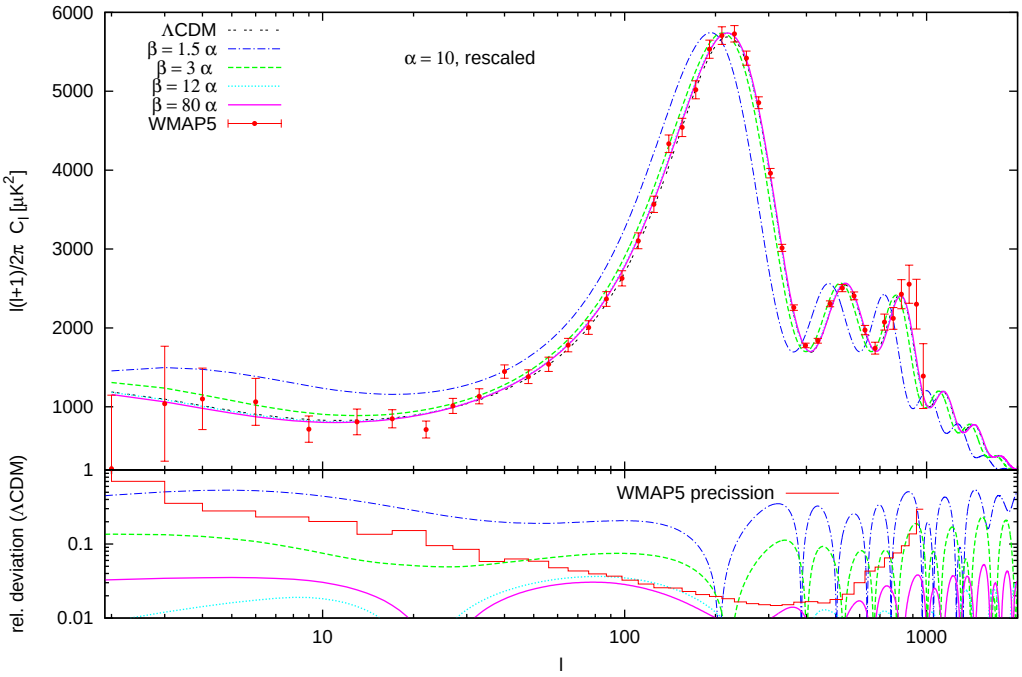

Figure 6.7: CMB spectra dependence on β/α ($\alpha = 10$). The lower part contains the residuals with respect to ΛCDM . Apart from the different choice in the initial amplitudes (see Figure 6.6) no other modification of the parameters has been performed. This shows the effect of modifying the angular distances, particularly noticeable for the curves with $\beta/\alpha = 1.5, 3$.

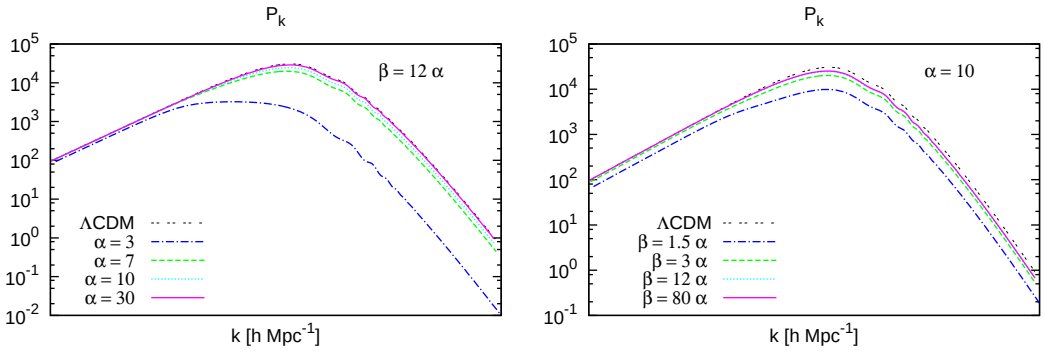

Figure 6.8: CDM spectra dependence on the parameters. This are the "raw" spectra evaluated at redshift zero. For a comparison with observational data see Figure 6.9.

6.3.2 Large Scale Structure

The disformal field is also likely to affect the way in which structure forms. The minimum expected effect is to inhibit structure formation to a certain extent by reducing the amount of cold matter at early times. Further effects may occur due to the clustering properties of the field. However, it seems unlikely to be significant on grounds of the behaviour of CMB spectra and since the interaction between matter and field occurs only indirectly via the gravitational potentials.

Figure 6.8 shows the parameter dependence of the cold dark matter power spectrum. It is seen how larger amounts of early dark energy, as well as lower equations of state (low α and β/α respectively) lead to lower values. However, comparison with astronomical data does not make use of this spectra, but rather a convolution using window functions and rescaled by a galaxy bias factor representing the efficiency of galaxy formation [55]. The plots in Figure 6.9 show how this "optimal spectra" have little dependence on α and none in β/α. However, the galaxy bias changes for the different models and becomes larger for the "less ΛCDM ". This deviations would become larger after the CMB rescaling mentioned in the previous section. Hence, any bound on the galaxy bias factor would allow CMB and LSS to put some constraints on *at least* the amount of early dark energy.

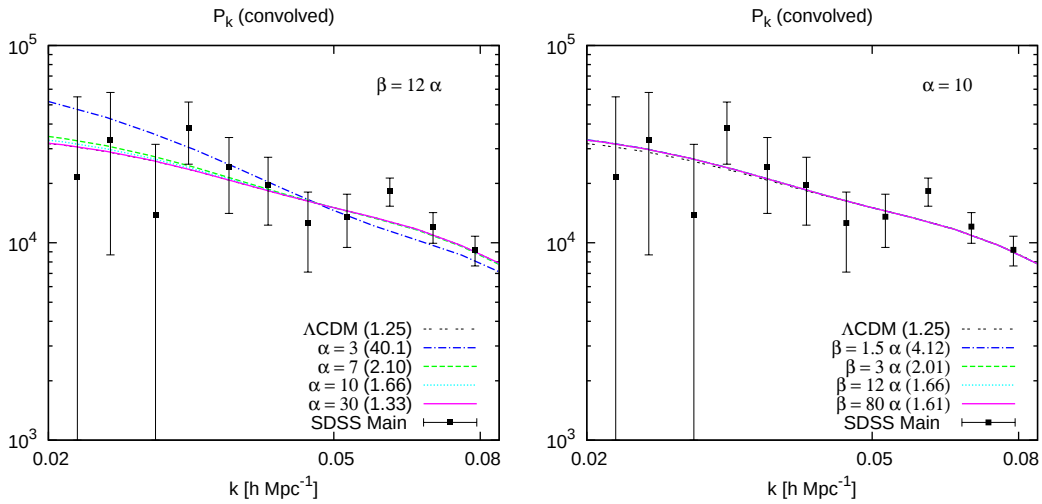

Figure 6.9: Corrected spectra to compare with the observed spectrum. The spectra at $z = 0.1$ are convoluted and corrected to galaxy formation by the CMBEasy analyse this class. Numbers in parenthesis correspond to the galaxy bias applied to correct each model (see text). Only values of k/h above the nonlinear threshold have been plotted. Black dots correspond to the SDSS main sample.

Chapter 7

Conclusions

The present work has considered a novel mechanism to trigger an accelerated expansion in the context of quintessence, namely the disformal effect. It is introduced in a rather simple way by postulating a second metric related to the gravitational one by a generalisation of the conformal relation. Unlike conformal metrics, the disformal case allows for a slow down of the time flow and can lead to and accelerated expansion in the late universe when applied to a cosmic scalar field.

This mechanism has been examined in detail within a simple setting. The model considers a minimally coupled field with an exponential potential in a flat FRW metric and introduces three free parameters. The good properties of quintessence such as the existence of scaling solutions remain unaffected and a very efficient transition into slow roll is achieved under appropriate conditions. The transition is particularly notable for the field equation of state which can change very quickly from zero to minus one. The role of the parameters has been examined, finding a limit in which the model is very likely to be indistinguishable from a cosmological constant.

Parameter constraints from astronomical data involving homogeneous behaviour were obtained. Type 1A supernovae, baryon acoustic oscillations and CMB shift parameter seem to favour a Λ-like behaviour, but the allowed parameter space is still large. In particular, no upper bounds were obtained for the additional parameters.

The equations for cosmological perturbations were obtained and the study of their behaviour was undertaken. This allowed an exam of how the disformal transition affected the perturbations and possible observational implications on the CMB anisotropies and LSS were also considered. At this stage of the research it does not seem clear to what extent the inclusion of linear perturbations will be able to improve the actual constraints. It further seems that the cosmological constant limit is also achieved at the perturbative level.

Disformal quintessence offers a good candidate for dark energy which can reproduce the effects of a cosmological constant. On the other hand, nothing within the model makes it more plausible than Λ and is has unfortunately been born in an epoch in

which quintessence has lost most of its popularity and glamour. However, old trends are known to come back and disformal quintessence has shown to be a patient field. It surely does not mind waiting for a better ocasion, as if time did not go by.

7.1 Perspectives

The present article depicts the actual state of a research with broader horizons. There are several things to be done in the near future and some ideas that showed up on the way and deserve to considered later on.

7.1.1 Perturbations and Full MCMC Analysis

The understanding of the perturbations carried away so far is still incomplete. The validity of first order perturbation theory would be doubtfull if the perturbed disformal factor becomes one for some mode. Certainly other aspects the perturbations need to be explored in more detail.

A complete MCMC study of the parameter space would then be carried out. Our actual computations render slow when perturbations are included and further work to make the code more efficient would certainly pay off.

New Datasets

Of course, further parameter constraints would benefit from search of optimal datasets. The inclusion of WMAP data is out of any doubt. Extra LSS data would be needed and a choice should be made among the available possibilities.

The main feature of the model is the occurrence of quick transition at high redshift. The constraints could be made tighter by including information about the Ly-α clouds, which provide information up to a very high redshift [56]. The drawback of this dataset is that it probes scales which are relatively small and for which dark energy is expected to be very diluted, but usefull background information may still be obtained.

A deeper exploration of the Hubble diagram could benefit from the inclusion of Gamma Ray Burst data as standard candle [57]. This bright objects are found up to $z \sim 10$ and if they become competitive standard candles would allow to explore a possible disformal transition in the late past.

Last, but not least, we would like to test disformal quintessence against the more modern BAO data of Percival et al. 07 [47] that was omitted in section 5.1.2. The information of the BAO scale at $z = 0.2$ seems to enter in contradiction with the standard cosmological model and it would certainly be interesting to know if disformal quintessence can do any better than Λ.

7.1.2 Related Models

It is conceivable that the variations obtained from table 4.1 are of some interest. Their analysis should be quite easy since all relevant equations have been calculated up to the sign of some terms. For example, phantom disformal quintessence might represent an interesting alternative with negative equation of state.

Applications of the Disformal Effect

Disformal quintessence is not only a model of dark energy. It is the application of a mechanism able to generate a very sharp transition under certain conditions. In this case disformal effect naturally lead to a transition in the equation of state of the scalar field, but it is possible to arrange it to achieve different effects in more sophisticated models.

Variations Within the Model

So far we have considered the case in which the conformal function was set to one. Interesting effects might arise for different choices of $A(\phi)$.

It might be easy and interesting to consider different choices for the potential and the disformal function. The condition $BV \sim 1$ needed to end the scaling regime makes reasonable to assume that $B(\phi)$ and $V(\phi)$ have similar functional forms and the choices are then reduced. Slower varying functions than the exponential might lead to tighter constraints.

Disformal Couplings

Disformal couplings to matter have been already explored in the literature. A funny variation would be to consider radiation in a disformal metric. Since conformal couplings of radiation reduce to usual ones, a term in the Lagrangian of the form

$$\frac{1}{4}\sqrt{\bar{g}}\bar{g}^{\alpha\beta}\bar{g}^{\gamma\delta}F_{\alpha\gamma}F_{\beta\delta} \tag{7.1}$$

might introduce new features and phenomenological challenges.

Appendix A

Partial Derivatives of the Lagrangian Density

In this appendix, the necessary derivatives of the Lagrangian density (equation 4.7 with $A(\phi) = 1$) used in chapters 4 and 6 are given.

$$p(\phi, X) = \frac{-X}{\sqrt{1 + 2B(\phi)X}} - \sqrt{1 + 2B(\phi)X}V(\phi)\Big). \tag{A.1}$$

$$p_{,X} = -\frac{1}{\sqrt{\mathcal{L}}}\left[1 + \frac{\mathcal{D}}{2\mathcal{L}} + BV\right] \tag{A.2}$$

$$p_{,XX}\dot{\phi}^2 = -\frac{\mathcal{D}}{\mathcal{L}^{3/2}}\left[2 + \frac{3\mathcal{D}}{2\mathcal{L}} + BV\right] \tag{A.3}$$

$$p_{,X\phi} = -\frac{1}{\sqrt{\mathcal{L}}}\left[\frac{\mathcal{D}_{,\phi}}{\mathcal{L}}\left(1 + \frac{3\mathcal{D}}{4\mathcal{L}} + \frac{1}{2}BV\right) + B_{,\phi}V + BV_{,\phi}\right] \tag{A.4}$$

$$p_{,\phi} = -\frac{1}{\sqrt{\mathcal{L}}}\left[\frac{\mathcal{D}_{,\phi}}{2}\left(\frac{X}{\mathcal{L}} - V\right) + \mathcal{L}V_{,\phi}\right] \tag{A.5}$$

$$p_{,\phi\phi} = -\frac{1}{\sqrt{\mathcal{L}}}\Big[\frac{(D_{,\phi})^2}{4\mathcal{L}}\left(\frac{3X}{\mathcal{L}} - V\right) - D_{,\phi}V_{,\phi} + \frac{\mathcal{D}_{,\phi\phi}}{2}\left(\frac{X}{\mathcal{L}} - V\right) + \mathcal{L}V_{,\phi\phi}\Big] \tag{A.6}$$

Appendix B

Disformal Quintessence in CMBEasy

CMBEasy [49] is an open source program for the computation of cosmological observables based on the popular CMBFAST [58]. It is written in C++, and its object oriented source code allows very clean modifications of the code by simply re-implementing the desired functions in the proper subclasses. As in its precursor, most quantities are stored in splines, a very efficient structure to contain and manipulate functions of a single variable. The actual version can compute power and CMB spectra, including tensor and polarisation within seconds. Two different gauges (synchronous and conformal newtonian) and several quintessence models are included. A typical CMB computation is done as follows:

1. The background and thermal histories are computed.
2. The perturbations are propagated in Fourier space.
3. The inhomogeneities are used to map the anisotropy spectrum seen today.

The *Analyze This!* [48] package provides the necessary functions to observationally constraint models. It is based on the `analizethis` class, containing the routines necessary to calculate the likelihoods of the computed model for a wide set of available astronomical data[1]. The analysis is completed with the `mc driver`, a program designed to run the MCMCs in a LAM/MPI parallel environment. In this setting, one computing (master) controls the exploration generates the points to be evaluated, computes the global statistics and sends the model parameters to the remaining processors (slaves), which return the corresponding likelihoods.

In addition, CMBeasy contains a graphic user interface that allows interactive computations and display of the results, as well as wide support to marginalise and represent the MCMC outputs.

[1]The actual version supports SNe, CMB, LSS, BAO, Lyα among others.

In order to perform the necessary computations we had to modify several classes in order to introduce the right quintessence model and modify the relevant equations. There were several issues we had to deal with in order to use disformal quintessence, from which we will sketch the most relevant.

B.1 Logarithmic Implementation

Most equations within the model contain products of very large and very small quantities, notoriously all quantities involving B_0. We noticed that the compiler treated this quantities as zero, even when they were multiplied by a correspondingly large factor. To avoid this, we constructed all the delicate functions ($B\dot{\phi}^2$, BV, $B_\phi V$ etc..) as first calculating the logarithm and then exponentiating. In this spirit, we used the variable $B_x \equiv \log(B_0)$ in these functions.

B.2 Forking Algorithm

As was mentioned in section 4.2.2, Ω_q is a growing function of $B_x \equiv \log(B_0)$. We made use of this fact to obtain the right B_x for any given cosmological parameters. First, the algorithm chooses an interval with the following steps

1. Run the cosmic history with $B_0 = 0$. This is equivalent to a normal quintessence that remains in the attractor (no acceleration) and set $B_x^{(0)} = -\beta\phi/M_p - \log(\dot{\phi})$ evaluated at $a = 1$.

2. Run the history with the value of $B_x^{(i)}$. If the obtained Ω_q is larger than the desired one, the interval is chosen to be $[B_x^{(0)}, B_x^{(i)}]$.

3. If Ω_q is lower than desired, B_x is shifted by $B_x^{(i+1)} = B_x^{(i+1)} + \beta/\alpha$ and step 2 is repeated.

Once the interval was chosen, a more precise numerical procedure already existent in CMBEasy was used to find the zero of $\Omega_q(B_x) - \Omega_q$ to desired accuracy.

B.3 Perturbations

We modified CMBEasy to use the equations derived from the previous section in the subclass that handles the perturbations in the synchronous gauge for quintessence scenarios (`quintsynchronous`). All partial derivatives of p appearing in the equations for the perturbations are background valuated. Therefore we computed them only once

together with the rest of the background history and stored them in splines that could be accessed by the integration routine for every k mode.

The program only uses the two first order equations (6.8,6.9) to calculate the evolution of the gravitational potential as well as the Klein Gordon equation for the field (6.28). This allowed us to use the pressure equation 6.10 as a consistency check, by constructing h'' numerically and comparing with the other terms. The test is nontrivial since it involves a differentiation.

We further checked against a third definition of the pressure obtained through the fluid formalism

$$\delta p_\phi = c_s^2 \delta\rho_\phi + 3\mathcal{H}(c_s^2 - c_a^2)(1 + w_\phi)\rho_\phi \frac{p_{,X}\phi'\delta\phi/a^2}{\rho_\phi + p_\phi} \tag{B.1}$$

where $c_a^2 = p'_\phi/\rho'_\phi$ and c_s^2 is given by (6.31).

Appendix C

Monte Carlo Markov Chains

When confronting cosmological models with observations, the objective is to determine which values of the free parameters (our theory) are compatible with an available set of astronomical data (our Universe). Since measurements are not infinitely precise, the compatible set of parameters will occupy a finite volume, which is unknown a priory.

What is known is the probability of obtaining a certain measurement for a given model. It can be obtained by comparing the theoretical prediction with the experimental value and its uncertainty. This probability is known as the the likelihood of observing X (a vector in the space of observations) given θ (a vector in the space of parameters). It has to be inverted in order to obtain the posterior distribution $\pi(\theta|X)$, i.e. the probability of θ being the true value if X is observed. Both probabilities are related through Bayes theorem:

$$\pi(\theta|X) = \frac{L(X|\theta)P(\theta)}{\int L(X|\theta)P(\theta)d\theta} \tag{C.1}$$

Monte Carlo Markov Chains constitute a widely used strategy to invert the likelihood and obtain the posterior distribution. A direct grid sampling of the parameter space requires a great deal of computational effort, since the number of points scales with exponentially with the number of parameters. On the other hand, MCMC execution times increase roughly linearly with the number of parameters.

A Markov Chain is a stochastic sampling of the parameter space $\{\theta_0, ..., \theta_n\}$ in which the point θ_i only depends on θ_{i-1}. If the way in which the chain is created is chosen properly, its distribution of the points will be the posterior distribution

$$\text{Dist}\{\theta_0, ..., \theta_n\} = \pi(\theta|X) \tag{C.2}$$

The sampling method used by CMBEasy is the Metropolis algorithm [59]. For a given point θ_i, the next point is chosen as follow:

1. Compute $L(X|\theta_i)$; the likelihood of observing X given the parameters θ_i.

2. Propose a new parameter vector by sampling from a proposal distribution $q(\theta_i, \theta_{i+1})$ (see below).

3. Compute the likelihood for the proposed parameter $L(X|\theta_{i+1})$.

4. If the likelihood is higher $L_{i+1} > L_i$, the point is added to the chain and the procedure goes to step 2.

5. If $L_{i+1} < L_i$, a random variable $u \in [0, 1]$ is generated. If $u < L_{i+1}/L_i$, the step is taken and go to 2. Otherwise go to 2, but reject the actual. θ_{i+1}.

The algorithm assumes flat priors $P(\theta)$ and a symmetric proposal distribution $q(\theta_i, \theta_{i+1})$. Likelihoods outside the boundaries are assigned zero likelihood.

An adaptive stepsize sampler helps to the convergence and mixing of the chains. Too large stepsize will lead to many steps being rejected, while too short stepsize will take a long time to sample the distribution. The function $q(\theta_i, \theta_{i+1})$ is Gaussian, and it is estimated from the previous points in the chains. Stepsizes are taking along the principal axes of this distribution to take into account the possible degeneracies among the parameters.

The initial point in the chain is chosen randomly in the parameter space and will move to regions of higher likelihood afterwards. Therefore, the first points in every chain do not reflect the distribution of $\pi(\theta|X)$. In order to test the convergency, the algorithm uses m chains to evaluate their mixing and convergence. CMBeasy uses the test of Gelman and Rubin [60] to calculate the variance of each parameter between chains. We denote by ψ_{ij} the value of one parameter at the point $j = 1, ..n$ of chain i, and a bar over a quantity means average over the missing indices. The variance between (B) chains and within (W) a given chain are given by

$$B = \frac{n}{m-1} \sum_{i=1}^{m} (\bar{\phi}_i - \bar{\phi})^2 \,, \tag{C.3}$$

$$W = \frac{1}{n} sum_{i=1}^{m} \frac{1}{n-1} \sum_{j=1}^{n} \,, \tag{C.4}$$

where the sums over the point index j are taken over the last n points instead of the whole chain. The quantity

$$R = \frac{\frac{n-1}{n} W + \frac{1}{n} B}{W} \tag{C.5}$$

should converge to one for the stationary distribution. If, for each parameter $R < 1.2$, the chain can be safely considered to be sampling from the posterior distribution.

Bibliography

[1] V. Mukhanov, *Physical Foundations of Cosmology* (2005).

[2] S. Dodelson, *Modern cosmology* (2003).

[3] S. M. Carroll, *Spacetime and geometry. An introduction to general relativity* (2004).

[4] A. H. Guth, prd **23**, 347 (1981).

[5] S. Weinberg, Rev. Mod. Phys. **61**, 1 (1989).

[6] R. Durrer and R. Maartens, Gen. Rel. Grav. **40**, 301 (2008), 0711.0077.

[7] E. Copeland, M. Sami, and S. Tsujikawa, International Journal of Modern Physics D **15**, 1753 (2006), URL doi:10.1142/S021827180600942X.

[8] J. Garcia-Bellido and T. Haugboelle (2008), arXiv/0802.1523.

[9] S. Perlmutter et al. (Supernova Cosmology Project), Astrophys. J. **517**, 565 (1999), astro-ph/9812133.

[10] A. G. Riess et al. (Supernova Search Team), Astron. J. **116**, 1009 (1998), astro-ph/9805201.

[11] S. Perlmutter, Physics Today **56**, 040000 (2003).

[12] B. Leibundgut, Gen. Rel. Grav. **40**, 221 (2008), 0802.4154.

[13] M. Kowalski et al. (Supernova Cosmology Project), Astrophys. J. **686**, 749 (2008), 0804.4142.

[14] J. Weller and A. M. Lewis, Mon. Not. Roy. Astron. Soc. **346**, 987 (2003), astro-ph/0307104.

[15] D. Eisenstein et al. (SDSS), Astrophys. J. **633**, 560 (2005), astro-ph/0501171.

[16] C. Wetterich, Nucl. Phys. **B302**, 668 (1988).

[17] B. Ratra and P. J. E. Peebles, Phys. Rev. **D37**, 3406 (1988).

[18] S. Tsujikawa, Physical Review D **73**, 103504 (2006), URL doi:10.1103/PhysRevD.73.103504.

[19] P. G. Ferreira and M. Joyce, Phys. Rev. D **58**, 023503 (1998).

[20] E. J. Copeland, A. R. Liddle, and D. Wands, Phys. Rev. D **57**, 4686 (1998).

[21] A. Albrecht and C. Skordis, Phys. Rev. Lett. **84**, 2076 (2000), astro-ph/9908085.

[22] T. Koivisto and D. F. Mota, Phys. Rev. **D75**, 023518 (2007), hep-th/0609155.

[23] T. Koivisto and D. F. Mota, Phys. Lett. **B644**, 104 (2007), astro-ph/0606078.

[24] L. Amendola, Phys. Rev. **D62**, 043511 (2000), astro-ph/9908023.

[25] T. Koivisto, Phys. Rev. **D72**, 043516 (2005), astro-ph/0504571.

[26] E. J. Copeland, N. J. Nunes, and F. Rosati, Phys. Rev. **D62**, 123503 (2000), hep-ph/0005222.

[27] T. Chiba, T. Okabe, and M. Yamaguchi, Phys. Rev. D **62**, 023511 (2000).

[28] C. Armendariz-Picon, V. Mukhanov, and P. J. Steinhardt, Phys. Rev. Lett. **85**, 4438 (2000).

[29] C. Bonvin, C. Caprini, and R. Durrer, Phys. Rev. Lett. **97**, 081303 (2006), astro-ph/0606584.

[30] S. M. Carroll, M. Hoffman, and M. Trodden, Physical Review D **68**, 023509 (2003), URL http://www.citebase.org/abstract?id=oai:arXiv.org:astro-ph/0301273.

[31] T. S. Koivisto, *Disformal quintessence* (2008), arXiv.org:0811.1957.

[32] V. Faraoni, E. Gunzig, and P. Nardone, Fund. Cosmic Phys. **20**, 121 (1999), gr-qc/9811047.

[33] J. D. Bekenstein, prd **48**, 3641 (1993), arXiv:gr-qc/9211017.

[34] J. D. Bekenstein, Phys. Rev. **D70**, 083509 (2004), astro-ph/0403694.

[35] M. Banados, A. Gomberoff, D. C. Rodrigues, and C. Skordis, Phys. Rev. **D79**, 063515 (2009), 0811.1270.

[36] M. Banados, P. G. Ferreira, and C. Skordis, Phys. Rev. **D79**, 063511 (2009), 0811.1272.

[37] A. Sen, JHEP **04**, 048 (2002), hep-th/0203211.

[38] A. Sen, JHEP **07**, 065 (2002), hep-th/0203265.

[39] A. Y. Kamenshchik, U. Moschella, and V. Pasquier, Phys. Lett. **B511**, 265 (2001), gr-qc/0103004.

[40] N. Kaloper, Physics Letters B **583**, 1 (2004), arXiv:hep-ph/0312002.

[41] C. Wetterich, Astron. Astrophys. **301**, 321 (1995), hep-th/9408025.

[42] J. S. Bagla, H. K. Jassal, and T. Padmanabhan, Phys. Rev. D **67**, 063504 (2003).

[43] D. Rubin, E. V. Linder, M. Kowalski, G. Aldering, R. Amanullah, K. Barbary, N. V. Connolly, K. S. Dawson, L. Faccioli, V. Fadeyev, et al. (Supernova Cosmology Project) (2008), arXiv.org:0807.1108.

[44] W. L. Freedman et al. (HST), Astrophys. J. **553**, 47 (2001), astro-ph/0012376.

[45] O. Elgaroy and T. Multamaki (2007), astro-ph/0702343.

[46] A. G. Sanchez and S. Cole, Mon. Not. Roy. Astron. Soc. **385**, 830 (2008), 0708.1517.

[47] W. J. Percival et al., Mon. Not. Roy. Astron. Soc. **381**, 1053 (2007), 0705.3323.

[48] M. Doran and C. M. Mueller, JCAP **0409**, 003 (2004), astro-ph/0311311.

[49] M. Doran, JCAP **0510**, 011 (2005), astro-ph/0302138.

[50] E. Komatsu et al. (WMAP), Astrophys. J. Suppl. **180**, 330 (2009), 0803.0547.

[51] J. Dunkley et al. (WMAP), Astrophys. J. Suppl. **180**, 306 (2009), 0803.0586.

[52] C.-P. Ma and E. Bertschinger, Astrophys. J. **455**, 7 (1995), astro-ph/9506072.

[53] J.-c. Hwang and H. Noh, Phys. Rev. **D66**, 084009 (2002), hep-th/0206100.

[54] E. V. Linder and G. Robbers, JCAP **0806**, 004 (2008), 0803.2877.

[55] M. A. Strauss et al. (SDSS), Astron. J. **124**, 1810 (2002), astro-ph/0206225.

[56] U. Seljak, A. Slosar, and P. McDonald, JCAP **0610**, 014 (2006), astro-ph/0604335.

[57] V. F. Cardone, S. Capozziello, and M. G. Dainotti (2009), 0901.3194.

[58] U. Seljak and M. Zaldarriaga, Astrophys. J. **469**, 437 (1996), astro-ph/9603033.

[59] N. Metropolis, A. W. Rosenbluth, M. N. Rosenbluth, A. H. Teller, and E. Teller, J. Chem. Phys. **21**, 1087 (1953).

[60] A. Gelman and D. B. Rubin, Statist. Sci. **7**, 457 (1992).

[61] H. Goldstein, C. Poole, and J. Safko, *Classical Mechanics*, vol. 2009 (2002), ISBN 0-201-65702-3.

[62] P. J. E. Peebles and B. Ratra, Rev. Mod. Phys. **75**, 559 (2003), astro-ph/0207347.

[63] P. S. Corasaniti, M. Kunz, D. Parkinson, E. J. Copeland, and B. A. Bassett, Phys. Rev. **D70**, 083006 (2004), astro-ph/0406608.

[64] P. Ruiz-Lapuente, Class. Quant. Grav. **24**, R91 (2007), 0704.1058.

[65] J.-c. Hwang and H. Noh, Phys. Rev. **D71**, 063536 (2005), gr-qc/0412126.

[66] F. Piazza and S. Tsujikawa, JCAP **0407**, 004 (2004), URL http://www.citebase.org/abstract?id=oai:arXiv.org:hep-th/0405054.